Review Article

INTERACTION OF IONIZING RADIATION WITH MATTER

James E. Turner*

Abstract—**The basic physical mechanisms by which different kinds of ionizing radiation interact with matter are described. Understanding of these processes, coupled with detailed knowledge of atomic structure, provides much of the foundation for the theory and practice of radiological health protection today.**

Health Phys. 86(3):228–252; 2004

Key words: radiation, ionizing; x rays; reviews; radiation protection

INTRODUCTION

THE ACCIDENTAL discovery of x rays by Röntgen on November 8, 1895, marked the introduction to mankind of a totally new and unexpected phenomenon in nature—ionizing radiation. The original findings were followed rapidly by the discovery of radioactivity and sources of ionizing radiation with properties different from those of x rays (Stannard 1988). Radiation research and use became intimately bound with the ever increasing understanding of its nature and its connection with atomic structure, atomic transitions, and the transmutation of chemical elements.

Radiation played a vital role in the unparalleled advances in science during the last century. Indeed, the enormous potential for medical applications of x rays was evident from the first investigations. As experience was gained in the early days, it became increasingly apparent that ionizing radiation can damage biological systems. In time, concepts and procedures were developed for protection around radiation sources, and laws were eventually enacted to control exposures of workers and the public to radiation. Today, many unique and important benefits to human life are realized through the utilization of radiation and its various sources. Work in radiation protection continues today on a large and active scale.

The size and scope of this scale increased by orders of magnitude in the 1940's with the formation of the Manhattan Project in the United States to construct the atomic bomb. As described by Karl Morgan (1967), it was a time "when it was difficult to anticipate the biological consequences of operating the large reactors and associated chemical plants that were to handle fission products in megacurie lots, quantities millions of times the number of curies of radium available to man in the entire world prior to the atomic age." The name "health physics" came out of this undertaking (Morgan 1967; Parker 1948; Kathren and Ziemer 1980; Taylor 1982), and the number of persons working in this profession continued to increase steadily after World War II. The Health Physics Society was founded in 1956, and the first issue of the journal *Health Physics* appeared in 1958.

The approaching 50th anniversary of the founding of the Health Physics Society affords an appropriate occasion to review and assess various components of the multifaceted profession of health physics. To this end, the present article has been prepared as a review on the subject of the physical interactions of radiation with matter. ("Radiation" will henceforth imply "ionizing radiation.") The basic mechanisms by which charged particles, photons, and neutrons interact with atoms, nuclei, and molecules will be described. Understanding of these processes is fundamental to dosimetry, instrumentation, shielding, and the interpretation of all manner of physical and biological effects produced by radiation. In a sense, each of these subjects begins as a "physics problem" at the level of an initial event that transfers energy from a radiation field to a material.

ATOMIC STRUCTURE

The ways in which radiation interacts with matter are reflected both in the nature of the radiation itself and in the structure of atoms. This relationship between "projectile" and "target" was exploited by Rutherford (1911) when he used alpha particles as a radiation probe to investigate the structure of the atom. His work led to the discovery of the nucleus. One can understand certain aspects of radiation penetration through matter by bearing in mind the special properties of the atomic target that is presented. A brief review of the Rutherford experiments will serve as a starting point for the present article.

* 127 Windham Road, Oak Ridge, TN 37830.
For correspondence or reprints contact J. E. Turner at the above address, or email at jamesturner17@comcast.net.

(*Manuscript received* 8 *October* 2003; *accepted* 13 *November* 2003)
0017-9078/04/0

At the time, the recognized properties of atoms were embodied in the structure proposed by Thomson. In his so-called "plum pudding" model, the electrically neutral atom was thought to consist of a number of electrons embedded in a continuous spherical distribution of an equal amount of positive charge, having a radius of $\sim 10^{-10}$ m. It was known that the alpha particle is an energetic, doubly ionized helium atom emitted spontaneously from some radioactive materials. It was also known that it is much more massive than the electron. Rutherford noticed that the angular deflections experienced by alpha particles traversing various materials were occasionally much larger than would be expected on the basis of Thomson's model. In a typical experiment (Geiger and Marsden 1909), a collimated pencil beam of 7.69-MeV alpha particles from ^{214}Po (RaC′) was normally incident on a gold foil, having a thickness of only $\sim 10^{-6}$ m. The foil was so thin that the particles lost only a small fraction of their energy in passing through it. The number of atoms traversed by a particle going through was about $10^{-6}/10^{-10} = 10^4$. As an ion, an alpha particle interacts with the charged components of the atoms via the long-range Coulomb force. The force is attractive for the negative, much less massive electrons and repulsive for the distributed positive charge of the Thomson atomic model. In traversing the foil, alpha particles in an initially collimated beam would accumulate a large number of small, random, back-and-forth deflections due to the Coulomb interactions. The beam would thus acquire a slight angular spread by the time it emerged from the other side of the foil. Some 99% or more of the exiting particles were observed to experience net deviations of less than 3°, with a root-mean-square spread of about 1°.

The statistical distribution of these small scattering angles was not in disagreement with expectations based on the Thomson model. What was at odds, however, was the occasional alpha particle that exited the foil at a large angle. One incident particle in about 8,000 was even scattered backwards from the foil. Although rare, such a happening simply could not be explained on the basis of the Thomson model. As Rutherford recounted years later (Rutherford 1938), "It was quite the most incredible event that has ever happened to me in my life. It was almost as incredible as if you fired a 15-inch shell at a piece of tissue paper and it came back and hit you. On consideration I realized that this scattering backwards must be the result of a single collision, and when I made calculations I saw that it was impossible to get anything of that order of magnitude unless you took a system in which the greater part of the mass of the atom was concentrated in a minute nucleus. It was then that I had the idea of an atom with a minute massive center carrying a charge." The scattering at large angles was brought about by a single, rare, close collision with a tiny, massive nucleus of positive charge at the center of the atom. Rutherford's calculated statistical distribution of particles scattered at both small and large angles based on the Coulomb force exerted by this nucleus agreed with the observed data. Moreover, the calculations were consistent with having the nucleus confined to a radius definitely less than 3×10^{-14} m, the distance of closest approach of the two like charges in a head-on collision. (Some interesting sites with interactive applets can be found on the World Wide Web by searching under "Rutherford scattering." See, for example, http://www.scri.fsu.edu/~jac/Java/rutherford.html).

It is well established today that the radius of the gold atom is 1.8×10^{-10} m and that of its nucleus is 7.6×10^{-15} m. The ratio of the atomic and nuclear diameters is, therefore, 24,000. Also, about 99.98% of the mass of the gold atom resides in this tiny nucleus. The radius of the alpha particle is 2.1×10^{-15} m. In discussing radiation interactions, it will be useful to keep in mind the rather extraordinary picture exemplified in Rutherford's experiments. It is hardly feasible to make a scale drawing of it here for this purpose. If one represented the gold nucleus by a dot having the diameter of a human hair ($\sim$0.007 cm), then the nuclear dot would be at the center of a sphere having a diameter of 170 cm, representing the size of the atom. The nearly invisible dot would also hold almost the entire mass of the atom. The vast volume surrounding the nucleus is "filled" by 79 electrons in rapid motion out to the dimensions of the sphere. Although a fast alpha particle passes readily through the space occupied by the atom, the atomic volume occupied by the electrons has structural integrity. Atoms in the foil strongly resist compression.

The next major advance in unraveling atomic structure was Bohr's semi-classical theory of the hydrogen atom (Bohr 1913b; Bohr 1913c). He postulated that its single atomic electron can move only in certain discrete, quantized orbits about the central nucleus. He postulated further that a photon in the spectrum of hydrogen is emitted when the electron makes a transition from one orbit to another of lower energy. There followed a decade of intense work to develop a semi-classical atomic theory, in which dynamic systems were approached classically with certain quantum rules imposed on them. Further understanding was gained, but these methods also led to many failures. Classical mechanics was proving to be incapable of describing the observed properties of atoms and radiation. The breakthrough came when Heisenberg (1925) proposed a radically different approach with a theory built on observable quantities. At about the same time and independently, Schrödinger (1926a, 1926b) proposed his wave equation, another revolutionary departure. These first papers in quantum

mechanics appeared in the mid 1920's. Although Heisenberg's matrix formulation and the Schrödinger wave equation are very different mathematically, the two theories were soon shown to be entirely equivalent (Schrödinger 1926c). To the question, "What is quantum mechanics?," Weisskopf (1989) has given the following response: "There is no doubt that the most outstanding development in modern science was the conception of quantum mechanics. It showed, better than anything else, the human capability to comprehend the fundamental principles that underlie the world in which we live—even when these principles run contrary to our experience in dealing with our everyday environment." Quantum mechanics revolutionized physics. It provides a powerful and highly successful theoretical framework today for treating not only the interaction of radiation with matter, but also all manner of properties observed in many diverse areas of physics, chemistry, and material sciences.

The subject of radiation interactions with matter can be conveniently divided into four general parts: the interaction of heavy charged particles, electrons and positrons, photons, and neutrons.

INTERACTION OF HEAVY CHARGED PARTICLES WITH MATTER

In this discussion, a *heavy charged particle* refers to any ion except an electron or positron, which are considered in the next section. The next massive particle after the electron is the muon, which has a rest mass 207 times that of the electron. The masses of all heavy ions are thus considerably larger than the mass of the electron.

Stopping power

A charged particle moving rapidly through matter loses energy primarily by ionizing and exciting atoms. An important goal of theoretical understanding of these processes is the prediction of the average rate of energy loss of the particle per unit distance traveled as a function of the particle's energy. This fundamental quantity is called the *stopping power* of the material for that particle. It is often denoted by the symbol $-\mathrm{d}E/\mathrm{d}x$ and expressed in the units MeV cm^{-1}. Dividing the stopping power by the density ρ of the material gives the closely related *mass stopping power*, $-\mathrm{d}E/\rho\mathrm{d}x$, which can be expressed in MeV $\mathrm{cm}^2\ \mathrm{g}^{-1}$.

At relativistic speeds, stopping power will depend on the speed, charge, and spin (if any) of a heavy ion and on properties of the medium. In the Rutherford experiments, the alpha particle's speed was considerably less than the speed of light. Its behavior is then governed by the long-range, electrostatic Coulomb force, which depends only on the separation between charges. Under these conditions, Bohr (1913a, 1915) made the first theoretical calculation of a stopping-power formula for a heavy ion, based on semi-classical physics, before the discovery of quantum mechanics. Detailed derivations of Bohr's formula are available in the literature (Turner 1967, 1995).

Bohr's semi-classical theory

Bohr treated the energy loss of an energetic, heavy charged particle due to collisions with individual atomic electrons. The occasional nuclear scattering as seen in Rutherford's experiments does not play a significant role in stopping power unless the ion is moving very slowly. Bohr assumed that an atomic electron can be considered approximately as free and at rest before the collision with the fast ion. Fig. 1 depicts the path of an ion, moving through a uniform medium with velocity V. It passes geometrically at a distance b, called the *impact parameter*, from electrons in a thin, annular cylindrical shell of thickness db and length dx. Since the ion is much more massive than the electrons it encounters, its path deviates negligibly from a straight line as it loses energy. Bohr also assumed that a struck electron in the annular shell moves only slightly in a short time, $t \sim b/V$, during which it feels the effective force exerted by the passing ion at its distance b of closest approach. If e denotes the electron's charge and ze the ion's charge, then the magnitude of the effective force F on the electron turns out to be just twice the Coulomb force (Turner 1995). Thus, $F = 2k_o ze^2/b^2$, where $k_o = 8.9876 \times 10^9\ \mathrm{N\,m^2\,C^{-2}}$. By Newton's second law, the momentum P transferred to the electron by the collision is the impulse, or product of the (constant) force and the time it acts,

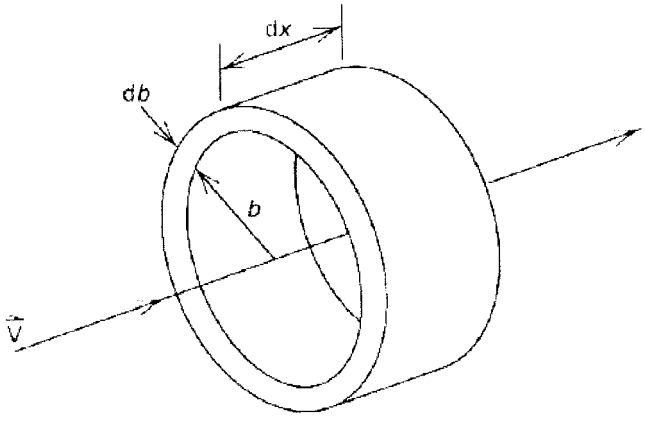

Fig. 1. Annular cylinder of thickness db and length dx centered along the path of a heavy ion, moving with velocity V through a uniform medium. (From James E. Turner, *Atoms, Radiation, and Radiation Protection*. Copyright 1995 by John Wiley and Sons, Inc. This material is used by permission of John Wiley and Sons, Inc.)

$$P = Ft = \frac{2k_o ze^2}{b^2}\frac{b}{V} = \frac{2k_o ze^2}{Vb}. \quad (1)$$

The energy acquired by the electron, and hence lost by the ion, is

$$Q = \frac{P^2}{2m} = \frac{2k_o^2 z^2 e^4}{mV^2 b^2}, \quad (2)$$

where m denotes the mass of the electron.

If the medium contains a uniform density of n electrons per unit volume then, in traveling the distance dx, the ion experiences $2\pi nb$ db dx collisions with impact parameter between b and b + db. Multiplication by Q gives for the energy loss of the ion to electrons in the shell when it traverses the distance dx,

$$-\mathrm{d}E = \frac{2k_o^2 z^2 e^4}{mV^2 b^2}(2\pi nb\ \mathrm{d}b\ \mathrm{d}x) = \frac{4\pi k_o^2 z^2 e^4 n}{mV^2}\frac{\mathrm{d}b}{b}\ \mathrm{d}x. \quad (3)$$

The linear rate of energy loss, or stopping power of the medium, is obtained by dividing by dx and integrating over impact parameters between the minimum and maximum possible values:

$$-\frac{\mathrm{d}E}{\mathrm{d}x} = \frac{4\pi k_o^2 z^2 e^4 n}{mV^2}\int_{b_{\min}}^{b_{\max}}\frac{\mathrm{d}b}{b} = \frac{4\pi k_o^2 z^2 e^4 n}{mV^2}\ln\frac{b_{\max}}{b_{\min}}. \quad (4)$$

Heuristic arguments can be used to set approximate limits for the integration. Under the principle of adiabatic invariance, recognized in semi-classical theory, the impulse on an atomic electron must be sharp in order to effectively induce a quantum transition to a higher-energy state. The duration of the collision must be less than the period $1/\bar{\nu}$ of an electron in the atom, where $\bar{\nu}$ denotes an average atomic frequency for this motion. Accordingly, $b/V < 1/\bar{\nu}$ is required for energy loss. This restriction implies an upper limit, $b_{\max} \sim V/\bar{\nu}$ for the impact parameter. At the lower end, it is assumed that the Coulomb force on the electron varies negligibly over its position. For this condition to be valid, the impact parameter for the collision must be larger than the de Broglie wavelength of the electron as "seen" by the ion. Since the electron has the speed V relative to the ion, its wavelength is h/mV, where h is Planck's constant. Therefore, $b_{\min} \sim h/mV$. With these limits substituted into eqn (4), one obtains the equivalent of Bohr's formula for a heavy charged particle moving with non-relativistic speed V in a uniform medium having n electrons per unit volume,

$$-\frac{\mathrm{d}E}{\mathrm{d}x} = \frac{4\pi k_o^2 z^2 e^4 n}{mV^2}\ln\frac{mV^2}{h\bar{\nu}}. \quad (5)$$

Bohr's intuitive semi-classical formula for the stopping power of a material has the same mathematical form as Bethe's quantum-mechanical formula, which is discussed next.

Bethe's quantum-mechanical theory

The relativistic quantum-mechanical stopping-power formula for heavy charged particles was derived by Bethe (Bethe 1930, 1933; Fano 1963). He calculated the differential cross section in the first Born approximation for the scattering of an ion from an initial to a final momentum state with simultaneous excitation of the atom from its ground state to an excited state. This cross section is integrated to obtain the total inelastic cross section for transitions of the atom to a given excited state. The stopping power is then proportional to the product of the inelastic cross sections and the excitation energies, summed over all final states of the atom. The result is

$$-\frac{\mathrm{d}E}{\mathrm{d}x} = \frac{4\pi k_o^2 z^2 e^4 n}{mc^2\beta^2}\left[\ln\frac{2mc^2\beta^2}{I(1-\beta^2)} - \beta^2\right], \quad (6)$$

in which $\beta = V/c$ is the ratio of the speed of the particle and the speed of light c. In the non-relativistic limit ($V \to 0$), it is seen that the Bethe and Bohr expressions for stopping power, eqns (6) and (5), become formally the same. The "average" atomic energy $h\bar{\nu}$ in the denominator of the logarithmic term in Bohr's formula (5) is seen in (6) to be replaced by another quantity I, called the mean excitation energy of the material. In contrast to $h\bar{\nu}$, this energy is defined explicitly in the quantum-mechanical theory as a weighted logarithmic mean over the excitation energies of the target atomic system (Fano 1963). I-values have been calculated theoretically for only a few atomic and molecular gases. In practice, they are obtained numerically from stopping-power measurements. Calculations based on the Thomas-Fermi statistical atomic model for an element with atomic number Z give the approximate result, $I \sim 10Z$ eV (Bloch 1933).

Fig. 2 shows the stopping power of liquid water for a number of heavy ions, electrons, and positrons as functions of particle energy. Except for electrons and positrons, the curves have been calculated from eqn (6) with various refinements, as discussed below. At high energies, the stopping power for a heavy ion shows a relativistic rise as $\beta \to 1$ in the denominator of the logarithmic term on the right-hand side of eqn (6). The rise is just discernible in the figure for the least massive

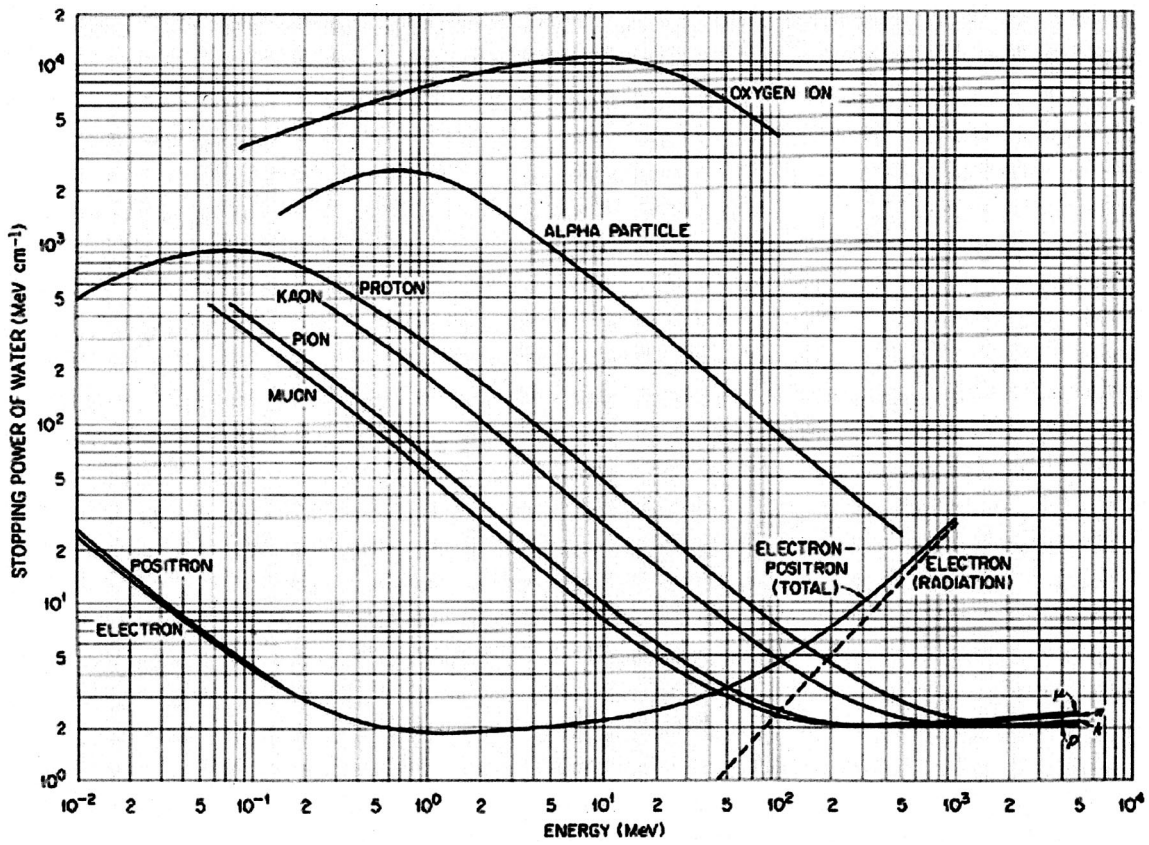

Fig. 2. Stopping powers of liquid water for various ions. (From James E. Turner, *Atoms, Radiation, and Radiation Protection*. Copyright 1995 by John Wiley and Sons, Inc. This material is used by permission of John Wiley and Sons, Inc.)

heavy ions, the muon and the pion. At decreasing energies, the stopping power increases because of the factor β^2 in the denominator outside the bracket. At still lower energies, β^2 in the numerator of the logarithmic term decreases rapidly, leading to a maximum value of the stopping power. Capture and loss of electrons from the medium also causes a decrease in the average charge of a positive ion and hence a decrease in the stopping power at low energies.

A number of compilations of heavy-ion stopping powers and ranges in various chemical elements, compounds, and mixtures are available in the literature. An extensive review of the subject and tables for protons and alpha particles have been published by the International Commission on Radiation Units and Measurements (ICRU) in ICRU Report 49 (1993a). Mass stopping powers and density ranges as well as other data are given for 26 elements and 48 other materials, many of particular importance for instrumentation, internal dosimetry, and other areas of health physics. The reader is also referred to the National Institute of Standards and Technology (NIST) Physics Lab Website (www.physics.nist.gov). The link to Physical Reference Data and then to Radiation Dosimetry Data provides the tabular information given in ICRU Report 49 as well as helpful graphs, not in the Report, and other information.

Generally, when numerical values cannot be found for a substance, one can apply the *Bragg additivity rule*. As a usually good approximation, the stopping power of a material can be approximated as the linear combination of the stopping powers for the elemental constituents, acting independently. Experimentally, chemical structure has about a 1% influence on stopping power (Fano 1963). The logarithm of the mean excitation energy I in eqn (6) is then the weighted average of the logarithms of the individual values I_i for the constituent atoms. That is,

$$n\ln I = \sum_i N_i Z_i \ln I_i, \tag{7}$$

when the material consists of N_i atoms per unit volume with atomic number Z_i, the sum being over all of the elements in the material. The mass stopping powers of materials of similar atomic composition are virtually the same numerically, as are the density ranges. For example, values for liquid water are approximately the same as

those for soft tissues, Mylar, Lucite, ferrous sulfate solutions (Fricke dosimeters), and even air. On the other hand, using water values on a density basis to approximate absorbers with high atomic number and tightly bound electrons, such as lead, seriously over-estimates mass stopping powers and under-estimates the density ranges.

The Bethe stopping-power formula is in excellent agreement with experiment over its range of applicability. Calculated in the first Born approximation, a theoretical condition for its validity is that the incident particle be moving much faster than the atomic electrons. This restriction fails at low ion energies and is not always met for inner-shell electrons in heavy elements. A positive ion, moving slowly through a medium, can also capture and lose electrons, thus proceeding with a variable charge to the end of its range. This effect occurs for alpha particles at about two MeV and below. In addition, as a heavy ion slows down, elastic scattering with atomic nuclei becomes important. Nuclear stopping powers, due to the Coulomb force between the ion and the nuclear charge screened by the atomic electrons, have been calculated. The nuclear and electronic stopping powers of liquid water for alpha particles, for example, are the same at about 3 keV (ICRU 1993a). Various theoretical and semi-empirical improvements have been made within the framework of eqn (6) to bring calculations and observations into satisfactory agreement at low energies. Still other considerations, such as collective effects and polarization in condensed media, also called the density effect, are not discussed here. Theory and experiment provide values of heavy-ion stopping powers above about 1 MeV with an accuracy approaching one percent (Fano 1963).

Scaling of stopping powers and ranges

It is of interest to examine the structure of eqn (6). As far as the properties of the heavy ion are concerned, the stopping power depends only on the charge, ze, and the velocity, $\beta = V/c$. The mass m is that of the struck electron. The properties of the medium that enter are the multiplicative density n of its electrons (trivial) and the mean excitation energy I (non-trivial). This mathematical structure implies certain scaling relationships between the stopping powers for different heavy charged particles, and hence their ranges also. According to eqn (6), the stopping power of a material for any two heavy ions, having the same charge and velocity, is the same. Also, if the speed is the same and the charges different, then the ratio of the stopping powers is equal to the square of the ratio of the charges. At the same velocity (relativistic or otherwise), the ratio of the kinetic energies of two particles is equal to the ratio of their rest masses. For example, a 6-MeV alpha particle ($z = 2$) and a 3-MeV deuteron ($z = 1$) have the same speed, since their mass ratio is two. The stopping power of a material for a 6-MeV alpha particle is thus four times that for a 3-MeV deuteron.

Ranges of heavy charged particles can also be scaled from one ion to another. The range $R(E_o)$ of a particle with initial kinetic energy E_o is defined as the mean distance it travels in a medium before coming to rest. In terms of the stopping power,

$$R(E_o) = \int_0^{E_o} \frac{dE}{-dE/dx}, \tag{8}$$

which has the dimensions of length. The quantity thus defined is the range calculated in the *continuous slowing-down approximation*, or simply the *csda range*. Eqn (8) treats slowing down as though it were a continuous, rather than discrete, process occurring at the mean rate $-dE/dx$. Multiplying the range by the density of a material provides a "*density range*," e.g., in g cm^{-2}. Expressed in this way, it represents the mass of an absorber per unit area that is traversed in stopping the particle. The density range of a material is independent of the actual density itself. For example, the density range for a gas is independent of the pressure.

For any heavy ion, the denominator of the integrand in eqn (8) is the stopping power. It can be written in the form $z^2G(\beta)$, where $G(\beta)$ is the universal function of velocity β implied by eqn (6) for any heavy ion. The relativistic kinetic energy E is equal to the rest mass M of the particle times another universal function of velocity. Therefore, in the numerator of the integrand in eqn (8) one can write $dE = Mg(\beta)d\beta$, where $g(\beta)$ depends only on velocity and is the same for all ions. Thus, if the variable of integration in eqn (8) is changed from E to β, then the range as a function of the initial velocity β_o can be expressed in the form

$$R(\beta_o) = \frac{M}{z^2}\int_0^{\beta_o} \frac{g(\beta)d\beta}{G(\beta)} = \frac{M}{z^2} f(\beta_o). \tag{9}$$

Although the function $f(\beta_o)$ cannot be evaluated in closed form, one knows from theory that it has the same value for any heavy ion with initial velocity β_o. It follows from eqn (9) that the ratio of ranges R_1 and R_2 for two ions, characterized by charges and rest masses z_1, M_1 and z_2, M_2, respectively, and having the same initial speed (same β_o), is

$$\frac{R_1(\beta_o)}{R_2(\beta_o)} = \frac{z_2^2 M_1}{z_1^2 M_2}. \tag{10}$$

As an example, the ranges of a deuteron (particle 1) and an alpha particle (particle 2) can be compared. The square of the charge ratio is $(z_2/z_1)^2 = 4$, and the mass ratio is $M_1/M_2 = ½$. Eqn (10) implies that the relation between the deuteron and alpha-particle ranges R_d and R_α is

$$R_d(\beta_o) = \frac{4}{2} R_\alpha(\beta_o) = 2R_\alpha(\beta_o). \quad (11)$$

Accordingly, starting with the same initial velocity, a deuteron travels twice as far in a material as an alpha particle. A 3-MeV deuteron has the same speed as a 6-MeV alpha particle, and so its range in a material is twice as large.

Due to the statistical nature of energy losses in slowing down, all heavy ions of a given type and with the same initial energy do not exhibit precisely the same distance of travel in coming to rest. This phenomenon is called *range straggling*. Because a large number of collisions are needed to stop an alpha particle, its straggling distribution of pathlengths is nearly Gaussian. The standard deviation is of the order of 1% of the mean range (eqn 8) in any material for most alpha emitters.

These scaling relationships for stopping power and range hold within the framework of the Bethe formula (eqn 6), which, as mentioned above, needs corrections under certain conditions. Uncertainties in stopping power below about 1 MeV, however, do not greatly affect ranges for energetic heavy ions.

Linear energy transfer

Stopping power is basically the same quantity as the *linear energy transfer (LET)* used in radiobiology and radiation protection (ICRU 1993b). In the latter context, LET usually refers to the stopping power of liquid water due only to electronic collisions and expressed in units of keV μm^{-1}. The concept of *restricted LET*, denoted by $(-dE/dx)_\Delta$, is also employed (ICRU 1980). It is the linear rate of energy lost in electronic collisions that includes energy losses only up to an energy cutoff Δ. For radiation-effects analysis, restricted LET makes a distinction, in principle, between the energy lost by an ion traversing a target (such as a sub-cellular constituent) and the energy actually absorbed in that target and thus not carried away by a secondary electron. One can see quite generally from Fig. 2 that the LET of charged particles increases with decreasing ion energy. LET has its maximum value near the very end of the particle's range. The alpha particle and oxygen ion are examples of high-LET ions; electrons and positrons have low LET. A proton can have high or low LET, depending on its energy.

Energy-loss spectrum

It remains to describe the spectrum of energy losses that a heavy charged particle experiences in a collision with an atomic electron. In the Bohr picture, a fast, heavy ion with mass M and kinetic energy E strikes an electron having mass m, considered free and initially at rest. In this approximation, the encounter with the unbound electron is elastic, and so the total kinetic energy and momentum of the two particles are conserved in the collision. Non-relativistically, the maximum energy that an incident particle of mass M can transfer to a struck particle of mass m is

$$Q_{max} = \frac{4mME}{(M+m)^2}, \quad (12)$$

which occurs in a head-on encounter. This relationship, which is demanded kinematically by the conservation laws, holds for any two masses M and m. For an incident alpha particle (M) and struck electron (m), the ratio of masses is $m/M = 1.4 \times 10^{-4}$. It follows from eqn (12) that an alpha particle can lose at most the fraction $Q_{max}/E = 5.6 \times 10^{-4}$ of its energy, or 0.056%. For a 4-MeV alpha particle, this amount is only 2.2 keV. Realistic calculations show that the most likely energy losses are far below this theoretical maximum.

Fig. 3 shows energy-loss spectra calculated for a 4-MeV alpha particle and, for comparison, a 1-keV electron in liquid water. The two are quite similar and characteristic of other charged particles. In most collisions, energy losses for either particle are in the range of a few tens of eV and seldom more than 100 eV. The distributions have tails, however, that extend on the right out to the maximum possible energy loss. Although relatively rare, the "hard" collisions represented in the tail contribute significantly to the stopping power, which

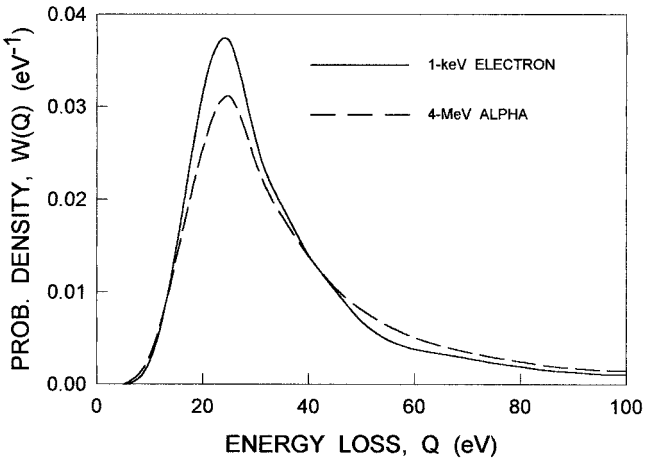

Fig. 3. Probability density function $W(Q)$ for energy loss Q by 1-keV electrons and 4-MeV alpha particles in liquid water.

is the integral over the collision cross section weighted by the energy loss. For example, calculations show that 1% of electrons at 1 keV in liquid water experience collisions in which $Q > 336$ eV (Turner et al. 1982). These collisions account for 10% of the stopping power for 1-keV electrons.

Using an estimate of 30 eV per collision as an average energy loss, one finds that roughly $(4 \times 10^6)/30 = 130{,}000$ collisions are needed to stop a 4-MeV alpha particle in a material.

Some health physics aspects

Some common and practical aspects of alpha radiation in health physics are readily linked to features of atomic structure and radiation interactions discussed here. As a ^{4}He nucleus traversing matter, an alpha particle experiences a large number of small energy losses in collisions with the much less massive electrons that occupy almost all of the volume. It travels almost in a straight path. Except for rare, large-angle nuclear scattering, alpha particles of a given energy have a well-defined range, with mean given by eqn (8) and a spread of the order of 1%. These characteristics of alpha tracks in tissue and other materials are in sharp contrast to those of beta particles, as will be described in the next section.

How far can an alpha particle penetrate in tissue? An estimate can be made based on Fig. 2. If the stopping power of a 6-MeV alpha particle, for instance, stayed constant as it slowed down, then the range in water (or soft tissue) would be (6 MeV)/(830 MeV cm^{-1}) = 7.2×10^{-3} cm = 72 μm. Since the stopping power actually increases as it slows down, a 6-MeV alpha particle will not travel this far. A better estimate of the penetration is obtained by approximating the average stopping power as that at the average energy, 3 MeV. The implied range is then roughly 40 μm, compared with the actual value, 50 μm (ICRU 1993a). Alpha particles and other heavy charged particles have short ranges and do not penetrate as far into matter as most other common radiations.

For radiation-protection purposes, the shallow dose equivalent for an individual is defined as that from external radiation at a surface depth of 0.007 cm, or 70 μm, corresponding to the nominal thickness used for the dead layer of skin. To penetrate to this depth, a normally incident alpha particle would need an energy of just under 7.5 MeV. Few alpha emitters are this energetic. Because of their short ranges, alpha particles cannot penetrate the dead layer of the skin, and so they are usually considered to present no hazard as external radiation. On the other hand, alpha emitters that are inhaled or ingested, or that enter the body through a wound, can damage living tissue as internal emitters. The validity of dosimetry models for alpha emitters in bone and soft tissues depends on an understanding of heavy-ion energy deposition on a microscopic scale. Models for the short-lived radon progeny in the lung have received special attention (NAS 1988).

The range of an alpha particle in water can also be used to estimate the range in other materials consisting of light elements. Air, for example, at standard temperature and pressure (STP) has a density $\rho = 1.29 \times 10^{-3}$ g cm^{-3}. The given range for a 6-MeV alpha particle in liquid water, 50 μm = 0.0050 cm, at unit density translates into a density range of 0.0050 g cm^{-2}. The estimated range in STP air is, therefore, (0.0050 g cm^{-2})/(1.29×10^{-3} g cm^{-3}) = 3.9 cm. The actual range is 4.5 cm (ICRU 1993a). The estimate in this case is only a fair approximation because the effective atomic number for air differs significantly from that for water.

A simple formula is sometimes useful for making a quick estimation of absorbed dose from exposure to a beam of heavy ions. Consider a uniform, parallel beam of ions of energy E with average fluence Φ that is normally incident on the plane surface of a target over an area A. The energy deposited by an ion over a small depth Δx from the surface into the target is $(-\mathrm{d}E/\mathrm{d}x)\Delta x$, where $-\mathrm{d}E/\mathrm{d}x$ is the average stopping power down to that depth. The total number of ions in the incident beam is ΦA. The total energy deposited in the volume behind A down to Δx is, therefore, $\Phi A(-\mathrm{d}E/\mathrm{d}x)\Delta x$. The mass of the material in the volume is $\rho A \Delta x$, where ρ is the density. The average absorbed dose in the surface volume is, therefore,

$$D = \frac{\Phi A\left(-\frac{\mathrm{d}E}{\mathrm{d}x}\right)\Delta x}{\rho A \Delta x} = \Phi\left(-\frac{\mathrm{dE}}{\rho \mathrm{d}x}\right). \qquad (13)$$

In other words, the dose per unit fluence, D/Φ, is equal to the mass stopping power of the material, $-\mathrm{d}E/\rho\mathrm{d}x$. In SI units, dividing the stopping power by the density gives directly (J m^{-1})/(kg m^{-3}) = J kg^{-1} m^2 = Gy m^2. One thus obtains the absorbed dose per particle per unit area.

It is well established in radiation biology that the same dose from different kinds of radiation can produce different degrees of biological damage. The effect of a given radiation type is usually compared with the effect of x rays in terms of its *relative biological effectiveness (RBE)*. This quantity is defined as the ratio of the doses needed from x rays and the given radiation to produce a specified biological effect. RBE is observed to depend on the biological endpoint under study, the radiation quality, dose level, dose rate, and other factors. Radiation quality, in turn, is often characterized by LET. For incident charged particles, the LET is that of the radiation itself.

For indirectly ionizing photons and neutrons, LET refers to that of the secondary charged particles they produce. Generally, RBE increases with increasing LET up to a point. Dense rates of energy deposition along the track of a particle per unit of energy deposited appear to be more damaging biologically than sparse deposition. The "optimal" value for many biological endpoints (e.g., cell killing) is in the range of 100 keV μm^{-1}. This finding has been linked to the fact that the average separation of ionization events at this LET is about the same as the diameter (2 nm) of the DNA double helix (Hall 2000). This circumstance would appear to favor the production of a double strand break from the passage of a single particle.

In applied health physics, alpha particles constitute high-LET radiation. In the units used in Fig. 2, this "optimal" radiobiological value of LET is 100 keV μm^{-1} = 1,000 MeV cm^{-1} in water. One sees that this is approximately the LET of a 4.4-MeV alpha particle. For radiation-protection purposes, alpha particles are assigned the largest *radiation weighting factor*, 20, on a scale from 1 to 20 for determining effective dose (ICRP 1991; NCRP 1993). (Historically, a quality factor of 20 is used for dose equivalent.)

INTERACTION OF ELECTRONS AND POSITRONS

This section describes the ways in which electrons and positrons interact with matter. There are many similarities between the two. The discussion will focus primarily on electrons, with differences being pointed out.

Stopping power

The linear rate of energy loss by a charged particle due to electronic collisions, like that described for heavy ions in the last section, is more precisely called the *collisional stopping power* of the medium. It can be symbolized by writing $(-dE/dx)_{col}$. Unlike heavy ions, electrons also lose energy by emitting electromagnetic radiation, called *bremsstrahlung*. The rate of energy loss by this mechanism is described by the *radiative stopping power*, $(-dE/dx)_{rad}$, which will be discussed below. The total stopping power of a material for electrons is the sum

$$-\frac{dE}{dx} = \left(-\frac{dE}{dx}\right)_{col} + \left(-\frac{dE}{dx}\right)_{rad}. \qquad (14)$$

When divided by the density of the absorber, these quantities are converted into the respective mass stopping powers. Also in contrast to heavy charged particles, electrons undergo considerable *elastic scattering* from atoms as they penetrate matter. They do not lose energy in this process, which therefore does not contribute to the stopping power. However, elastic scattering results in changes in the direction of travel.

Collisional stopping power

Like a heavy charged particle traversing matter, an electron loses energy through the electromagnetic forces experienced in collisions with atomic electrons, resulting in ionizations and excitations. However, there are several reasons why the heavy-ion stopping-power formula (6) cannot be applied to the collisional stopping power for electrons (Fermi 1960). It was assumed that the heavy ion is not deflected appreciably when it imparts momentum to an atomic electron, and hence it continues to travel almost in a straight line. The component of momentum received by the incident ion in the direction perpendicular to its path is approximately the same as the momentum imparted to the atomic electron. For a massive incident ion, this momentum change can cause only a slight deflection. For an incident electron with its small mass, on the other hand, the deflection can be large. Also unlike a heavy ion, an incident electron can lose a large fraction of its kinetic energy in a single collision with the atomic electron, a target having the same mass. These considerations apply to incident positrons as well.

Incident electrons are, if fact, *identical particles* with respect to the atomic electrons with which they collide. Therefore, quantum-mechanical exchange effects for these spin-1/2 particles must be taken into account. In place of the non-relativistic eqn (12), the exact relativistic expression for the maximum energy loss under the same initial conditions is

$$Q_{max} = \frac{2\gamma^2\beta^2 mc^2}{1 + \frac{2\gamma m}{M} + \left(\frac{m}{M}\right)^2}, \qquad (15)$$

where $\gamma = 1/\sqrt{1-\beta^2}$ is the usual relativistic factor. Setting the mass of the incident particle equal to that of the electron, $M = m$, one obtains from eqn (15) $Q_{max} = (\gamma - 1)mc^2$. The last quantity is equal to the kinetic energy T of the incident ion, so that $Q_{max} = T$. Thus, the incident particle could lose its entire energy in a head-on collision, like two billiard balls. However, when two electrons collide, because they are identical particles one cannot determine experimentally which of the two that emerge from the collision should be designated as the incident electron. (This is not the case for incident positrons.) By convention, the stopping power is calculated for the more energetic of the two emerging electrons. This condition restricts the maximum energy loss for the incident electron to be $T/2$, or one-half the incident energy. For the distinguishable incident positron, the maximum energy loss is T.

The collisional stopping power for electrons was also calculated by Bethe in the first Born approximation. The result is (ICRU 1984)

$$\left(-\frac{dE}{dx}\right)_{col} = \frac{2\pi k_o^2 e^4 n}{mV^2}\left[\ln\frac{mV^2T}{2I^2(1-\beta^2)} - (2\sqrt{1-\beta^2}-1 + \beta^2)\ln 2 + 1 - \beta^2 + \frac{1}{8}(2-2\sqrt{1-\beta^2}-\beta^2)\right]. \quad (16)$$

All of the symbols have the same meaning as before. (A similar expression, which differs in detail after the leading logarithmic term, applies to positrons.) Fig. 2 shows the total stopping power of water for electrons and positrons as a function of energy. The curves for the two types of radiation are indistinguishable at energies above about 200 keV and only slightly different below. As with heavy ions, the stopping power decreases with increasing energy and then exhibits a relativistic rise as $\beta \rightarrow 1$. The rise begins at considerably lower energies for electrons than for heavy charged particles. The radiative stopping power (due to bremsstrahlung) of water for electrons (shown by the dashed line in Fig. 2) is important at high energies. It is equal to the collisional stopping power of water at about 95 MeV. At higher energies, the linear rate of radiative energy loss exceeds that of the collisional loss. In materials of high atomic number, the two rates are equal at much lower energies.

Radiative stopping power

According to classical physics, when accelerated, an ion with charge ze and mass M will radiate energy as electromagnetic waves. The radiation is called bremsstrahlung, another name for continuous x radiation. In a single encounter the ion can lose any amount of energy from zero up to its total kinetic energy. The amplitude of the radiation is proportional to the acceleration a. As an ion of mass M passes a nucleus with charge Z at a distance r, it experiences a Coulomb force, which by Newton's second law gives the relationship, $k_o zZe^2/r^2 = Ma$. The acceleration of the ion at a distance r is thus proportional to zZe^2/M. The intensity of the radiation is proportional to the square of the product of the amplitude and the ion's charge. The intensity of the bremsstrahlung, in turn, is then governed by the proportionality

$$(zea)^2 \propto \frac{z^4Z^2e^6}{M^2}. \quad (17)$$

It follows that the total bremsstrahlung per atom varies from element to element as Z^2, the square of the atomic number, and depends inversely on the square of the mass M of the incident ion. The inverse dependence on M^2 accounts for the fact that bremsstrahlung for heavy charged particles is negligible compared with that for electrons. The ratio of the alpha-particle and electron masses is 7,300. At the same speed and distance in the same material, an alpha particle would produce on the order of 10^{-8} as much bremsstrahlung as an electron.

The classical and quantum-mechanical mechanisms for bremsstrahlung are different. According to quantum mechanics, each time a charged particle is deflected, there is a small probability that a photon will be emitted. When emission does occur, the radiated photon has a relatively large amount of energy. This emission of radiation, which is consistent with experiment, is in contrast to the classical theory in which there are a large number of small energy losses. The average bremsstrahlung energy losses in the quantum and classical pictures are comparable.

Radiation can also occur when an incident electron is deflected by an encounter with an atomic electron. The ratio of cross sections for electron-electron and electron-nucleus bremsstrahlung is small at low energies and increases steadily with increasing energy, becoming greater than unity at several tens of MeV.

The difference in the sign of the electric charge of electrons and positrons leads to some differences in their bremsstrahlung. At low energies, the cross sections for positron-nucleus radiation are smaller than those for electron-nucleus. At high energies, there is little electron/positron difference in the cross sections for either nucleus or electron bremsstrahlung. Additional information is given in ICRU (1984).

Extensive studies and numerical calculations have been made on many aspects of bremsstrahlung for electrons and positrons. There are no simple formulas available for radiative stopping power, analogous to eqn (16) for collisional stopping power. A valuable compilation of numerical data for bremsstrahlung by electrons and positrons in the form of extensive tables for a number of elements has been made by Seltzer and Berger (1986). As a rule of thumb, the ratio of the radiative and collisional stopping powers of an element with atomic number Z for electrons of kinetic energy T MeV is roughly

$$\frac{(-dE/dx)_{rad}}{(-dE/dx)_{col}} \cong \frac{ZT}{800}. \quad (18)$$

Range

The range of an electron as a function of energy can be defined as the csda range, eqn (8), just as for a heavy charged particle. In this case, the total stopping power for the electron applies in eqn (8). However, one should bear in mind that, typically, a heavy ion of a given type and energy will travel a distance close to the csda range in an

almost rectilinear path. It loses energy in small amounts, and the number of collisions needed to stop it is large. The stopping distances of monoenergetic heavy ions cluster around the value of the csda range. Electrons exhibit quite different behavior. They are frequently scattered at large angles, and their paths are far from rectilinear except at high energies. Electrons can lose a large fraction of their energy in single collisions with atomic electrons, which have the same mass. As a result, under otherwise identical conditions, electrons show a wide variation in the paths they take and in the distances they travel before stopping. Because of its relationship to the total stopping power, the csda range (8) provides the *mean distance* that electrons of initial energy E_o travel. The spread of this distribution for electrons is much larger than that for heavy ions. Because their paths in a target are tortuous, relatively few electrons penetrate to a depth equal to their range. Unless otherwise qualified, "range-energy" tables for electrons give csda ranges.

ICRU Report 37 (1984) furnishes a comprehensive review of the subject of electron and positron stopping powers. Like the companion ICRU Report 49 (1993a) on protons and alpha particles, it gives extensive numerical tables for stopping power and ranges for a large number of elements, compounds, and mixtures. The tables give collisional, radiative, and total mass stopping powers as well as csda density ranges from 10 keV to 1 GeV. Radiation yields (the average fraction of the initial energy of an electron that is converted into bremsstrahlung as the electron stops) and density-effect corrections are also included. The reader is referred again to the NIST Physics Lab Website (www.physics.nist.gov), which has the data in ICRU Report 37 on line. In addition, data can be calculated on the Website for electrons in any user-specified material.

Electron tracks in water

Further insight into the characteristics of electron penetration in matter can be gotten from computer simulation models that generate individual electron tracks. Perhaps most useful for this purpose are Monte Carlo codes, which carry out event-by-event collisions for an electron, transporting a primary and all of its secondaries until they come to rest. Interaction cross sections, energy-loss probabilities, angular scattering distributions, and other data are provided as input files for such a code. Experimentally measured data are used whenever available, supplemented with theoretical values. The input files enable the computer program to calculate the transport of an electron based statistically on the selection of random numbers. The goal is to program electrons on the computer to behave statistically like they do in nature. A number of codes, developed independently at different laboratories, have been used for studies in dosimetry, microdosimetry, radiochemistry, and biological-effects modeling.

The author has been involved with the development of one such computer code, called OREC, for electron transport in liquid water (Ritchie et al. 1991). This code, which computes the transport of electrons in liquid water, has been substantially revised recently and renamed NOREC (Semenenko et al. 2003). As an example, Fig. 4 shows a complete track calculated with NOREC for a 10-keV electron and all of its secondaries stopping in liquid water. Each dot represents the location of an initial species that ionizing radiation produces in water. These are either (1) an ionized water molecule, H_2O^+; (2) an excited water molecule, H_2O^*; or (3) an electron with too little energy to produce additional species. They are formed very rapidly, in $\sim 10^{-15}$ s in local regions of a track, where subsequent chemistry develops. By design, the Monte Carlo simulation keeps account of the identity of all species, their locations, and the energy deposited there.

The 10-keV primary electron in Fig. 4(a) starts out at the coordinate origin (0, 0, 0) moving initially along the positive X axis. Its increasing LET as it slows down is evident from the progressively increasing density of the dots. The clustering of events as an electron stops has received special attention in studies of "end-of-track" biological effects, particularly for low-energy electrons. A delta ray was produced about midway along this particular track. It was created by a relatively rare collision in which the transfer of energy is sufficiently large to enable the struck electron to make an identifiable track of its own, distinct from that of the primary. In (b), the track is viewed by looking downward in the negative direction parallel to the Z axis onto the XY plane. The electron very early veers away from the X axis. The view in (c) is parallel to the positive X axis in the direction of the initial travel. As the electron slows down, its path becomes more tortuous. Toward the end, elastic scattering with short mean free paths dominates an electron's behavior, which becomes diffusive-like in character.

By comparison, tracks for heavy ions crossing a region of water on the scale of Fig. 4(a) are straight and much more heavily populated with dots. Depending on the specific conditions, the density of dots can typically be one or two orders of magnitude greater than for electrons. Both types of particle interact with the medium through the Coulomb force and produce the same initial species. However, their patterns of energy deposition are quite different, presumably with different implications for the subsequent chemical and biological changes induced in an irradiated system.

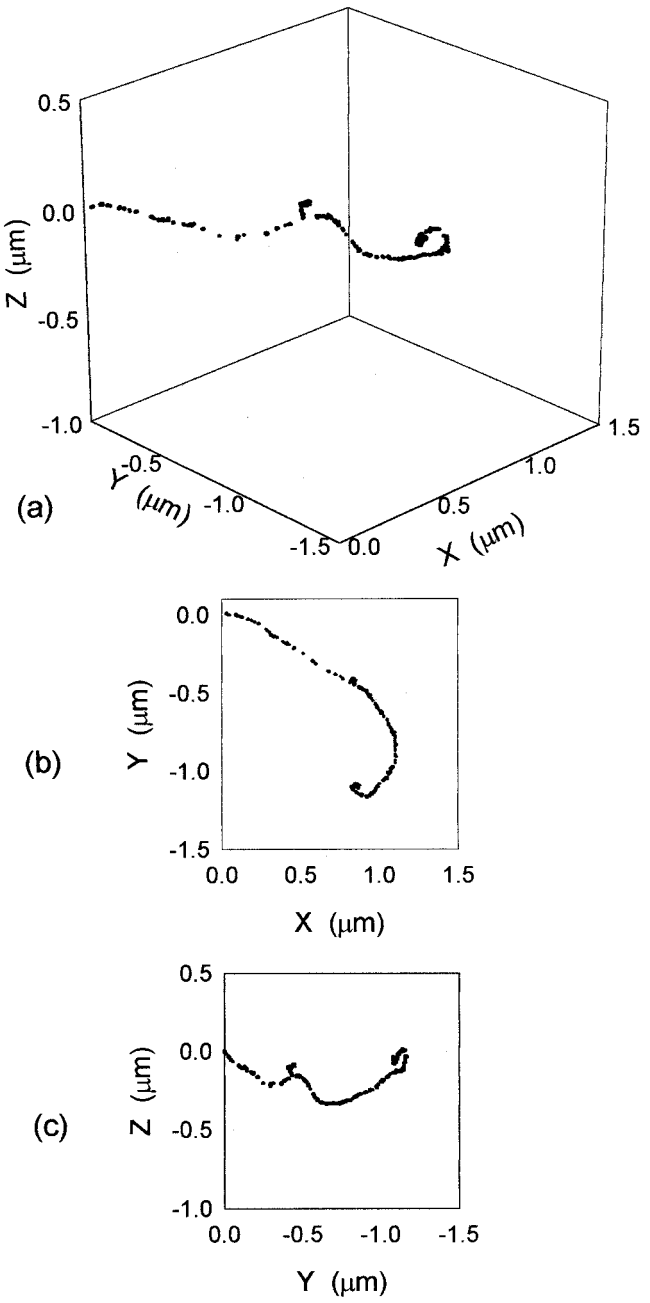

Fig. 4. (a) Three-dimensional representation of the complete track calculated for a 10-keV electron and all of its secondaries in liquid water. The electron starts out at the coordinate origin (0, 0, 0) in the direction of the positive X axis. Each dot shows the location of an ionized or excited water molecule or a sub-excitation electron. A short delta ray can be seen about midway along the track. (b) Projection of track on the XY plane. (c) Projection on YZ plane.

Some health physics aspects

Alpha particles are usually not considered to be an external radiation hazard. All but very soft external beta radiation, on the other hand, can penetrate the body to reach the depths of living tissue. An electron with 65 keV of energy has a range in water equal to the regulatory "shallow dose-equivalent" depth of 0.007 cm. The range of a 740-keV electron in water is 0.3 cm, the tissue depth used for dose equivalent assessment for the lens of the eye. In principle, particles from a pure beta emitter (no accompanying gamma radiation) can be shielded completely by a thickness of material equal to the range of the particles of maximum energy. However, in so doing, the additional consideration of bremsstrahlung from the beta rays slowing down in the shield is introduced. To minimize its generation, consistent with eqn (17) the shield should consist of low-Z material, such as plastic. A layer of high-Z material, like lead, can be used outside the plastic to efficiently shield the bremsstrahlung. Interchanging the order of the two materials, however, could substantially reduce their effectiveness.

The values quoted above for the tissue depths at the two energies are the csda ranges from ICRU Report 37 (1984). As Fig. 4 illustrates, beta particles do not travel in straight lines. For a number of practical reasons, shielding and dosimetry among them, the idea of expressing beta-particle range as a function of initial electron energy warrants further consideration.

Repeated Monte Carlo calculations of tracks like that carried out for Fig. 4 indicate that electron tracks come in a wide variety. Fig. 5 displays results compiled statistically from a sample of 10^7 independent, random histories calculated for 10-keV electrons in water. Shown are the probability density functions for the distributions of pathlength and maximum depth of penetration. Electrons start out the same as in Fig. 4. The pathlength is the total distance covered by a primary electron along the

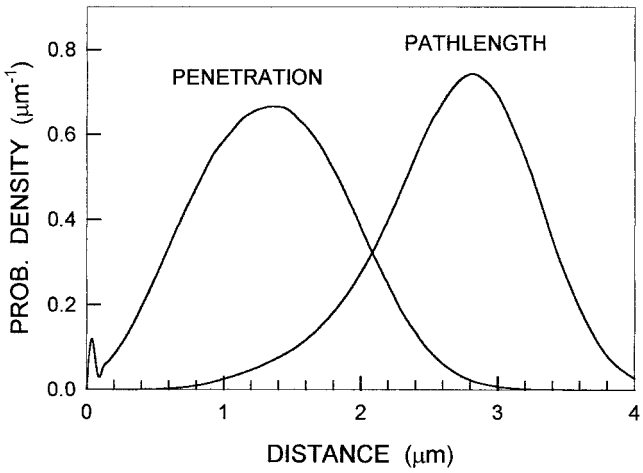

Fig. 5. Results of Monte Carlo calculations of the probability density functions for the distributions of pathlength and maximum depth of penetration for a sample of 10^7 10-keV electrons in liquid water. Geometry is the same as that for the electron in Fig. 4. Penetration depth was calculated with vacuum assumed in the space $x < 0$.

particular path that it travels. The penetration depth is the largest value of x that is reached. In Fig. 4(b), for instance, the penetration depth is seen to be about 1.1 μm. The pathlengths of electrons in Fig. 5 vary considerably out to a distance of more than 4 μm, while relatively few electrons reach beyond 3 μm. The average pathlength is 2.62 μm, and the average penetration depth is 1.31 μm. The mean pathlength is the same quantity as the csda range, which is given in ICRU Report 37 as 2.52 μm.

Backscatter from the water target was registered in the computer program whenever a primary electron first crossed the YZ plane into the space $x < 0$. The maximum depth of penetration for that electron was then scored as the largest previous value, $x > 0$, that it had. The computation of its transport was still continued as though it were in an infinite water medium in order to compile its contribution to the pathlength distribution in Fig. 5. The structure at the lower left of the penetration curve appears to be real, reflecting the distribution of depths reached by electrons that are backscattered. Under the given initial conditions, every electron has its first collision on the positive X axis. Backscatter in the computations was 8%.

Qualitative features seen in Fig. 5 persist up to the region of 1 MeV and even beyond. Calculations indicate that the average maximum depth of penetration is roughly one-half the csda range (Turner et al. 1988; Semenenko et al. 2003). Relatively few electrons reach a depth equal to the csda range. With energies of tens of MeV, electrons exhibit characteristics of beams.

External beta-ray dosimetry presents formidable technical problems. The radiation produces steep and nonuniform dose gradients in tissue and in the sensitive volumes of instruments. The only precise and absolute measurement of beta dose in a tissue-equivalent phantom is accomplished with the extrapolation chamber (ICRU 1997). Calculations are an important part of beta dosimetry (Durham and Bell 1992; NCRP 1999).

INTERACTION OF PHOTONS

Photons and quantum electrodynamics

X- and gamma-ray photons are familiar to health physicists. But what are they, and what do they do to matter? They are electromagnetic radiation, which, under various experimental conditions, exhibits dual properties of waves and particles. A gamma photon emitted from a ^{137}Cs source, for example, has an energy $E = h\nu = 0.662$ MeV $= 1.06 \times 10^{-13}$ J, where $h = 6.626 \times 10^{-34}$ J s is Planck's constant and $\nu = 1.60 \times 10^{20}$ s^{-1} is the frequency of the radiation. The wavelength is $\lambda = c/\nu = 1.88 \times 10^{-12}$ m, the quantity $c = 3.00 \times 10^{8}$ m s^{-1} being the speed of light in a vacuum. The photon has zero mass. Its momentum is $P = h\nu/c = 3.53 \times 10^{-22}$ kg m s^{-1}, consistent with the de Broglie relationship $\lambda = h/P$ between the wave-like property λ and the particle-like property of momentum. This gamma ray, like all photons, carries one unit of angular momentum, $\hbar = h/2\pi$ J s. It is thus a "spin-1" boson. The radiation is also characterized by polarization. This last property describes the time dependence of the electric field-strength vector as the transverse electromagnetic wave propagates.

Photons are quantum mechanical in nature. It is a general feature of quantum field theories that a particle of specific mass and spin is associated with every field. The photon is the field quantum of the electromagnetic interaction. Photons appear and disappear as quantum-mechanical excitations of the electromagnetic field, and they can be regarded as particles with mass zero and spin one.

In classical physics of the late 19th century, the description of electricity and magnetism rested on the highly successful Maxwell equations and their prediction of electromagnetic wave radiation. Originally unsuspected, the discontinuous nature of radiation energy was first inferred by Planck around 1900, in his study of the spectral distribution of black-body radiation. It was also employed by Einstein in his 1905 explanation of the photoelectric effect. All evidence since then has consistently confirmed the fact that energy exchanges between atoms and electromagnetic radiation are always discrete and obey the relationship $E = h\nu$.

Following the initial papers in quantum mechanics, Dirac (1928) proposed his famous relativistic equation for the electron. Electron spin and states of negative energy thus emerged as a requirement of relativity in quantum mechanics. Subsequent work addressed the interactions of electrons with electromagnetic radiation in various degrees of approximation. Today, quantum electrodynamics, which entails quantization of the electromagnetic and Dirac fields (second quantization), furnishes a rigorous and complete description of the interaction between photons, electrons, and other charged particles. The Coulomb force between two charged particles results from the exchange of virtual photons between the two. Virtual photons are emitted for very short periods of time, consistent with the uncertainty principle that relates time and energy. They do not permanently escape and are not directly observed. Their exchange accounts for the properties seen in charged-particle and photon interactions. The long range of the Coulomb force (compared, for example, with the nuclear force) is a consequence of the zero mass of the photon. As one of the major contributors to its development,

Feynman (1985) has written, "The theory of quantum electrodynamics has now lasted for more than fifty years, and has been tested more and more accurately over a wider and wider range of conditions. At the present time I can proudly say that there is *no significant difference* between experiment and theory."

Photon penetration in matter

Being electrically neutral, a photon does not experience Coulomb forces at large distances that almost constantly reduce its energy as it traverses matter in the way that a charged particle does. What is observed is that a photon of given energy in a uniform medium proceeds with a certain probability per unit distance of having an interaction or collision. This probability is called the *linear attenuation coefficient*, μ, of the medium for photons of that energy. It has the dimensions of inverse length, e.g., cm^{-1}. The quantity μ is also called the *macroscopic cross section*. If the density of the medium is ρ, the penetration can also be characterized by the *mass attenuation coefficient*, μ/ρ, e.g., with units $cm^2\ g^{-1}$. A photon is either absorbed or scattered by an interaction.

The behavior for uncollided photons is described by the familiar exponential attenuation function. If a narrow beam of N_o monoenergetic photons enters a uniform absorber having attenuation coefficient μ, then the number $N(x)$ that are still in the beam at a depth x without having interacted is

$$N(x) = N_o e^{-\mu x}. \quad (19)$$

The "survival" probability $e^{-\mu x}$ for the uncollided photons with distance x is analogous to the "survival" probability $e^{-\lambda t}$ in time t for undecayed radionuclides with decay constant λ. Like the mean life $1/\lambda$ for radioactive decay, $1/\mu$ is the average distance that incident photons travel before interacting, also called the *mean free path* or *relaxation length*. The exact exponential attenuation expressed by eqn (19) is due to the fact that photons in the narrow beam are removed by single scattering or absorption events. The attenuation coefficient governs the passage of photons through matter. Unlike charged particles, photons have no associated range that limits their distance of travel. According to eqn (19), there is always a finite probability that some incident photons will get through a shield of any thickness without having an interaction.

In most health physics applications that involve x or gamma rays, at least one of three principal interaction mechanisms with atoms plays an important role. These will be described next. Each has its own individual attenuation coefficient, and their sum is μ. Two elastic (coherent) processes, Rayleigh and Thomson scattering, are usually of minor concern and will not be covered. Photon absorption by atomic nuclei also occurs but will not be discussed. These cross sections are usually much smaller than those for the three principal interactions. However, bremsstrahlung around high-energy electron accelerators produces neutrons through (γ,n) nuclear reactions.

Photoelectric effect

In the photoelectric process, an incident photon with energy $h\nu$ is absorbed by an atom. The photon disappears, and an electron is ejected from the atom. The electron emerges with kinetic energy $T = h\nu - B$, where B is the binding energy of the electron in one of the states of the atomic shell, K, L, . . ., from which it came. An unbound electron cannot absorb a photon, because this process cannot simultaneously conserve momentum and energy. Binding of the electron and exchange of momentum with the rest of the atom are essential in order for the photoelectric effect to occur.

Photoelectric absorption is the dominant mode of attenuation for low-energy photons (several tens or hundreds of keV, depending of the atomic number of the absorbing atoms). At the lowest energies, ejection of an outer-shell electron might be the only event energetically possible. With increasing energy, the photoelectric attenuation coefficient for an element shows abrupt rises at the energies where ejection of an electron from an inner shell or subshell becomes energetically possible. These rises are seen as the familiar K, L, . . . edges in the attenuation coefficients for elements of middle and high atomic number.

Theoretical calculations for the photoelectric effect are difficult and involved. Analytic expressions for interaction cross sections, such as those for charged particles, are not readily available. In general, photoelectric attenuation coefficients vary as some (non-integral) power of the atomic number Z, around the range of four. The dependence on photon energy approximates the inverse cube. Thus, photoelectric attenuation coefficients for elements are, very roughly, proportional to $Z^4/(h\nu)^3$ (Evans 1955).

Compton scattering

Whereas the photoelectric effect accounts for most of the attenuation of low-energy photons, its influence falls rapidly with increasing energy. At the same time, the probability for Compton scattering of a photon increases. Compton scattering is the dominant mode of attenuation from intermediate energies to beyond the threshold (1.022 MeV) for pair production, discussed in the next section.

In a simplified treatment, a photon with energy $h\nu$ and momentum $h\nu/c$ collides with an atomic electron.

The latter is considered to be free and initially at rest (as in the Bohr semi-classical computation of stopping power). The photon is scattered at an angle θ with respect to its original direction of travel, and the struck electron recoils with kinetic energy T at another angle. As a result of the collision, the photon has less energy and momentum than before, the difference being transferred to the electron. Independently of the details of the mechanism of Compton scattering, the conservation of total energy and momentum provides useful relationships between the partners after the interaction. The kinetic energy of the struck electron is given by

$$T = h\nu \frac{1 - \cos\theta}{\frac{mc^2}{h\nu} + 1 - \cos\theta}. \quad (20)$$

The electron receives the maximum energy when the photon is scattered in the backward direction. With $\theta = 180°$, this energy is

$$T_{\max} = \frac{2h\nu}{2 + \frac{mc^2}{h\nu}}. \quad (21)$$

In principle, these and other relationships derived from the conservation laws need corrections due to the binding of the atomic electron, which was assumed to be free. In practice, however, at low energies where the corrections might be appreciable, photoelectric absorption is typically a much more important interaction.

The energy of the scattered photon is

$$h\nu' = \frac{h\nu}{1 + \frac{h\nu}{mc^2}(1 - \cos\theta)}. \quad (22)$$

At increasingly high energies, the energy of the back-scattered photon thus approaches the value $h\nu' = mc^2/2 = 0.256$ MeV. A remarkable feature of the scattering observed by Compton is that the shift $\Delta\lambda$ in wavelength between the incident and scattered photons seen at any given angle is independent of the incident-photon energy. The conservation laws show that

$$\Delta\lambda = \frac{h}{mc}(1 - \cos\theta) \quad (23)$$

for all incident energies. The constant, $h/mc = 2.426 \times 10^{-12}$ m, is called the *Compton wavelength*. It is the wavelength of a photon with energy equal to the rest energy $mc^2 = 0.5110$ MeV of the electron.

Whereas the incident photon can be scattered in any direction θ from 0° to 180°, the electron is always scattered in the forward direction, between 0° and 90°. The angular distribution for the scattered photons is given by the Klein-Nishina formula (Klein and Nishina 1929). The agreement achieved with experiment represents one of the earliest triumphs of Dirac's relativistic theory of the electron.

Pair production

The highly successful Dirac equation (Dirac 1928, 1958) implies that electrons have states of negative total energy. Since an excited state has a finite lifetime, the familiar electrons in positive-energy states that are observed all around should spontaneously make transitions to states of negative energy with the emission of photons. Faced with this dilemma, Dirac suggested that all of the negative-energy electron states in nature must already be occupied under normal conditions. Then the Pauli exclusion principle, which says that no two electrons can occupy the same state, would prevent the transitions from happening. A vacuum must actually be an infinite sea of electrons in completely filled states of negative energy.

While an electron in a positive-energy state cannot emit a photon and make a transition to an occupied state of negative energy, it should be possible for an electron with negative energy to absorb a photon and be promoted to positive energy. Since the initial total energy of the promoted electron is equal to or less than $-mc^2$ and the final energy is equal to or greater than $+mc^2$, the threshold photon energy required for the reaction is $2mc^2$. Absorption of such a photon creates a "hole" in the negative-energy electron sea. The energy of the sea is that of the vacuum minus the negative energy of the vacated electron state, which is a positive quantity. Furthermore, the hole exhibits a positive charge, $-(-e) = e$, equal in magnitude to that of the electron, but of opposite sign. The absence of the negative-energy electron thus appears as the presence of a particle with positive charge. It turns out, also, that the mass of the positive particle has to be the same as the electron mass, m. At the time of Dirac's proposal, the existence of the positron, which was discovered in 1932, was still unknown.

Absorption of a photon by an electron in a negative-energy state is called pair production. A photon with energy $h\nu \geq 2mc^2 = 1.022$ MeV disappears, and an electron-positron pair appears with particle kinetic energies T_- and T_+. The photon energy is converted into the total energy of the pair:

$$h\nu = 2mc^2 + T_- + T_+. \quad (24)$$

The conversion represented by this equation is strictly applicable when pair production takes place in the field of a heavy charged particle. Its presence is necessary for the conservation of momentum. An atomic nucleus, for

example, absorbs a negligible, but essential, amount of recoil momentum without appreciably changing (eqn 24). The energy of the positron or electron in eqn (24) can have any value between zero and $h\nu - 2mc^2$. Total charge is automatically conserved by the mechanism of pair production.

Pair production can also take place in the field of atomic electrons, though the probability is much less than that for a nuclear field. In this case, there are two electrons and one positron present after the transition, which is sometimes referred to as "triplet" production. The threshold energy is $4mc^2$.

The inverse process of electron-positron annihilation happens when a positive-energy electron makes a transition to fill a hole in the normally filled negative-energy sea. Annihilation photons are observed around radioactive positron sources. Emitted positrons rapidly stop in matter and annihilate with an electron. Two 0.511-MeV photons are then emitted back-to-back.

Interaction coefficients

The linear attenuation coefficient, μ, which governs the penetration of monoenergetic x and gamma rays incident on a uniform medium according to eqn (19), is the sum of the attenuation coefficients for the three types of interactions just described. Denoting the attenuation coefficients for photoelectric absorption, Compton scattering, and pair production, respectively, by τ, σ, and κ, one writes

$$\mu = \tau + \sigma + \kappa. \tag{25}$$

The same relationship holds between the mass attenuation coefficients for the different mechanisms. Fig. 6 shows the relative importance of the three interactions at different energies in different elements. The lines are drawn at the values of Z and $h\nu$ for which the probabilities for the two adjacent effects are equal. As already mentioned, the photoelectric effect is the most important for low energies and high Z. At intermediate energies the Compton effect is the dominant mode of attenuation for all Z. Pair production dominates at high energies and large Z. For compounds and mixtures of materials, the attenuation coefficients are assumed to be the sum of the individual, independent atomic contributions.

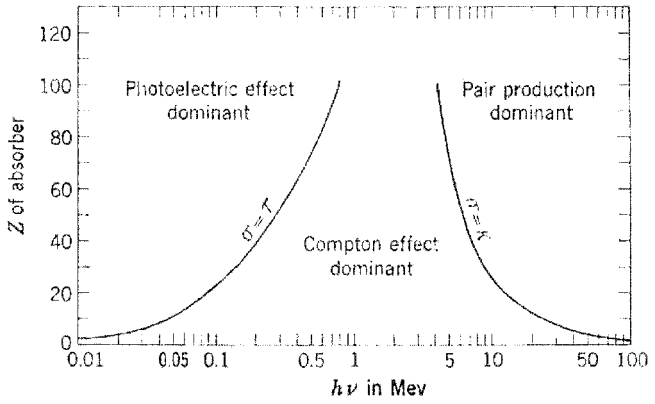

Fig. 6. Relative importance of photoelectric effect, Compton scattering, and pair production at different photon energies hν in elements of different atomic number Z. Lines show the locus of points at which $\sigma = \tau$ and $\sigma = \kappa$. (From Robley D. Evans, *The Atomic Nucleus*, copyright 1955. Published by McGraw-Hill and used by permission of the McGraw-Hill Companies.)

For dosimetry, one often needs to assess the energy transferred or energy absorbed in a material exposed to photons. While the attenuation coefficient describes the local *removal* of photons from a beam, it does not directly provide a measure of the resulting energy *transferred* to the target or *absorbed* around the removal site. The *energy transfer coefficient*, μ_{tr}, is defined as the product of the attenuation coefficient and the average fraction of the energy of the removed photon that is transferred as initial kinetic energy to secondary charged particles. This coefficient is defined next for each of the three principal photon-interaction mechanisms.

When a photon of energy $h\nu$ is photoelectrically absorbed, an electron is ejected with initial kinetic energy $T = h\nu - B$, where B is the binding energy that the electron had in the atom. The vacancy left in the atom, usually in the K or L shell, is followed by rearrangement of the electrons within the atomic shells. Rearrangement commences with an electron from a higher shell making a transition to fill the vacancy created in the inner shell. This can happen in two ways. Either a photon is simultaneously emitted from the atom as fluorescence radiation or else a series of Auger electrons is emitted. The former process does not contribute to the energy-transfer coefficient, by definition, because that energy is not transferred to secondary charged particles. The latter, Auger, process does contribute to the value of the energy-transfer coefficient, essentially with the amount of energy B. If δ represents the average energy released as fluorescence radiation per photoelectric event, then the fraction $\delta/h\nu$ of the incident photon's energy is not imparted to secondary electrons. The energy transfer coefficient for photoelectric absorption is, therefore,

$$\tau_{tr} = \tau\left(1 - \frac{\delta}{h\nu}\right). \tag{26}$$

For Compton scattering, the energy transfer coefficient is given by

$$\sigma_{tr} = \sigma\frac{T_{avg}}{h\nu}, \tag{27}$$

where $T_{avg}/h\nu$ is the average fraction of the photon energy that is transferred to the Compton electron. The average energy of the Compton electron, T_{avg}, is obtained from eqn (20) by averaging T over all angles θ of the scattered photon. In this case the energy taken from the incident photon and not imparted to secondary electrons is scattered and transported away from the interaction site as a photon with reduced energy. The Compton-scattering attenuation coefficient, obtained by averaging the scattered-photon energy in eqn (22), is

$$\sigma_s = \sigma \frac{(h\nu')_{avg}}{h\nu}. \quad (28)$$

The Compton attenuation coefficient is the sum of the energy-transfer and scattering coefficients:

$$\sigma = \sigma_{tr} + \sigma_s. \quad (29)$$

When pair production takes place in a nuclear field, an electron-positron pair is created with initial kinetic energy $h\nu - 2mc^2$, according to eqn (24). The energy-transfer coefficient is then

$$\kappa_{tr} = \kappa\left(1 - \frac{2mc^2}{h\nu}\right). \quad (30)$$

This relationship neglects the small contribution from energy transfer by triplet production. Also, positrons that annihilate in flight lead to a slight decrease in the value implied by eqn (30).

The total linear energy-transfer coefficient μ_{tr} for photons of energy $h\nu$ in a uniform absorber is the sum of eqns (26), (27), and (30):

$$\mu_{tr} = \tau\left(1 - \frac{\delta}{h\nu}\right) + \sigma\frac{T_{avg}}{h\nu} + \kappa\left(1 - \frac{2mc^2}{h\nu}\right). \quad (31)$$

To a good approximation this quantity determines the conversion of incident-photon energy into kinetic energy of secondary electrons and positrons in an absorber. Also included is the average energy of Auger electrons following photoelectric absorption.

One further refinement is needed in order to obtain the energy absorbed, as opposed to the energy transferred, especially for high-Z materials and high photon energies. Bremsstrahlung from the secondary charged particles (electrons) transports energy away from a local region and is not considered in the energy-transfer coefficient. If g represents the average fraction of the initial kinetic energy of the charged particles that is subsequently radiated as bremsstrahlung, then the *energy-absorption coefficient* is defined as

$$\mu_{en} = \mu_{tr}(1 - g). \quad (32)$$

Mass energy-absorption coefficients are useful for calculating the absorbed dose delivered by photons.

Fig. 7 shows these various linear attenuation coefficients and the energy-absorption coefficient as functions of photon energy for liquid water, which closely approximates soft tissue. Comparison with Fig. 6 reveals how the different interactions combine at different energies to determine the overall penetration in the low-Z medium. At intermediate energies, between about 0.1 MeV and 6 MeV, Compton scattering accounts for virtually all of the attenuation. In this region, therefore,

$$\mu = \sigma = \sigma_{tr} + \sigma_s, \quad (33)$$

in accord with eqns (25) and (29). In addition, one sees that $\mu_{en} = \sigma_{tr}$, because little bremsstrahlung is produced in water by Compton electrons in this energy range. Energy absorption is due almost entirely to Compton scattering, and the difference between μ and μ_{en} is due to Compton-scattered photons. The contributions of σ_{tr} and σ_s are the same in water at around 1.5 MeV.

Numerical values of photon coefficients can be obtained from a number of sources (e.g., Attix 1986; Shleien et al. 1998; Hubbell 1999). The NIST Physics Lab Website, mentioned before, has the following description of the tables there: "Tables and graphs of the photon mass attenuation coefficient μ/ρ and the mass energy-absorption coefficient μ_{en}/ρ are presented for all of the elements $Z = 1$ to 92 and for 48 compounds and

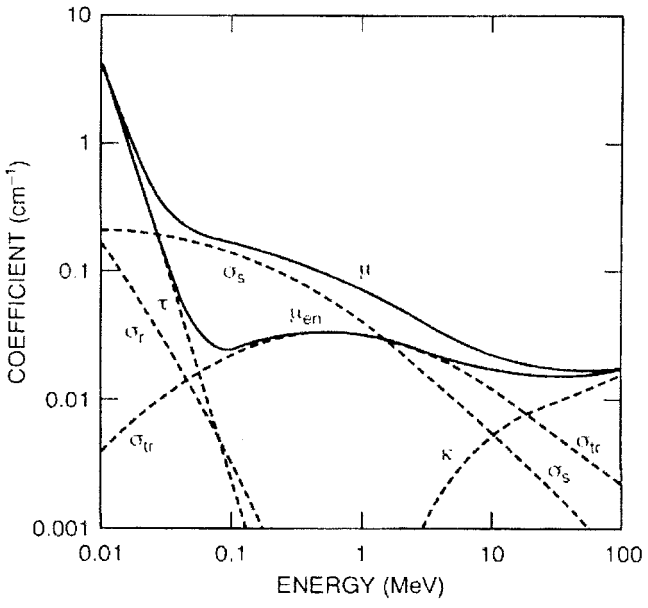

Fig. 7. Linear attenuation coefficients and energy-absorption coefficient as functions of energy for photons in water. (Attenuation coefficient σ_r for Raleigh scattering is included for comparison.) (From James E. Turner, *Atoms, Radiation, and Radiation Protection*. Copyright 1995 by John Wiley and Sons, Inc. This material is used by permission of John Wiley and Sons, Inc.)

mixtures of radiological interest. The tables cover energies of the photon (X-ray, gamma ray, and bremsstrahlung) from 1 keV to 20 MeV."

Some health physics aspects

Shielding calculations are carried out to determine the thickness of material needed to reduce a given photon field to some desired level. Computations can also be made to determine how much a given shield reduces the radiation. In either setting, the problem can be related to the linear attenuation coefficient μ and eqn (19) in the following way.

Consider an experiment in which a steady, narrow beam of monoenergetic photons is incident on a small counter placed some distance away. A uniform shield in the form of a broad slab of thickness x is placed near the source in such a way that the photon beam is normally incident on it. The shield reduces the count rate to a level $e^{-\mu x}$ of what it was without the shield. [This arrangement is called "good," or "narrow-beam," geometry (Cember 1996; Turner 1995).] Consider next a second experiment, which is like the first except that the narrow beam is replaced by a broad, parallel beam of photons of the same energy (an example of "poor" geometry). The count rate is, of course, again reduced relative to what it would be in the broad beam without the shield. However, the relative count rate is now larger than $e^{-\mu x}$. The same shield thickness is less effective in attenuating the broad beam. The difference is caused by photon scattering in the shield. In the first experiment, only uncollided photons reach the counter. In the second experiment, the counter registers not only the uncollided photons, as before, but also photons scattered into it from various points in the shield. The radiation transmitted with a broad beam is greater than that implied simply by the linear attenuation coefficient.

The transmission of electromagnetic radiation through shields under conditions of "poor" geometry can be formulated approximately in terms of a buildup factor, B. If the intensity of the incident radiation (e.g., J s^{-1} m^{-2} = W m^{-2}) on a shield is I_o and the intensity of the transmitted radiation is I, then one writes

$$I = BI_o e^{-\mu x}, \tag{34}$$

where μ is the linear attenuation coefficient. The buildup factor is thus seen to be the ratio of total transmitted intensity I (uncollided primary plus scattered photons) and the intensity of the uncollided primary radiation alone. B is never less than unity. Buildup factors have been determined for a number of different materials, different source and shield geometries, and different photon energies. They also depend on the specific quantity under consideration, such as intensity, exposure, or absorbed dose.

In another application, the mass energy-transfer coefficient μ_{tr}/ρ is closely related to the concept of *kerma* (**k**inetic **e**nergy **r**eleased per unit **m**ass). Kerma is defined as the initial kinetic energy of all secondary charged particles liberated per unit mass at a point of interest by uncharged radiation (ICRU 1980; Attix 1986). It is applicable to photons and neutrons and has the same units, J kg^{-1} = Gy, as absorbed dose. To see the relationship with μ_{tr}/ρ, let Ψ (J m^{-2}) be the energy fluence of monoenergetic photons passing normally over an area A in an absorber. Then the energy transferred to charged particles in a volume over a short distance dx behind the area is $\Psi A \mu_{tr} dx$. Since the mass in the volume with density ρ is $\rho A dx$, the kerma is

$$K = \frac{\Psi A \mu_{tr} dx}{\rho A dx} = \Psi\left(\frac{\mu_{tr}}{\rho}\right). \tag{35}$$

Therefore, the kerma is simply the product of the energy fluence and the mass energy-transfer coefficient.

The photon interactions discussed here allow for the interpretation of detailed features seen in pulse-height spectra. It is instructive to examine a measurement presented by Evans (1972) of pulses from the 662-keV ^{137}Cs gamma rays, shown in Fig. 8. [The photons are actually released by the transition of the metastable (half-life 2.55 min) ^{137m}Ba daughter nucleus of ^{137}Cs to its ground state.] The data were taken with a 4 × 4 inch NaI(T1) crystal. The total energy peak is due to pulses caused whenever the entire energy of an incident photon is absorbed in the crystal. This can happen in two ways. First, a primary photon is photoelectrically absorbed, and the photoelectron, Auger electrons, and fluorescence radiation are all absorbed in the crystal. Second, it can result from an incident photon that is Compton scattered one or more times before being photoelectrically absorbed in the crystal. Either way, a pulse is registered in the vicinity of 662 keV. There is an inherent spread in the width of the total energy peak because of statistical fluctuations in the conversion of the absorbed radiation energy into the number of electrons in the external circuit that registers the pulse. (The resolution is expressed as the full width of the peak at one-half its maximum value relative to its mean.) The Compton edge represents the maximum energy that an electron can acquire from Compton scattering by a primary photon. From eq. (21) with $h\nu$ = 662 keV and mc^2 = 511 keV, it follows that T_{max} = 478 keV, as seen in Fig. 8. Pulses registered above this value are due partly to the finite resolution of the counter and to multiple Compton scattering of an

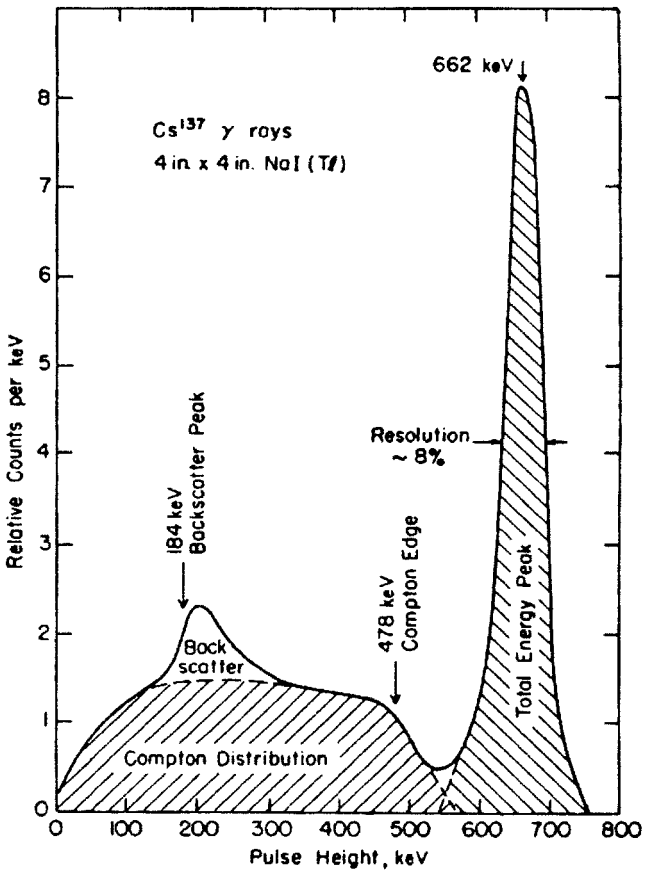

Fig. 8. Pulse-height spectrum measured with 4 × 4 inch NaI(T1) crystal scintillator exposed to gamma rays from ^{137}Cs. See text for details. (From Robley D. Evans, "Gamma Rays," in Dwight E. Gray, ed., *American Institute of Physics Handbook*, 3rd Ed., copyright 1955. Published by McGraw-Hill and used by permission of the McGraw-Hill Companies.)

incident photon. Two or more Compton recoil electrons can contribute more energy than T_{max}. Below the Compton edge is a continuum of pulses, mostly from single or multiple scatterings with $T < T_{max}$. The backscatter peak results not from directly incident primary photons, but rather from photons that are scattered into the scintillator from the surrounding neighborhood. These photons have been scattered mainly through large angles. Since eqn (22) with 180° gives $h\nu' = 184$ keV for the energy of a backscattered photon, one would expect this peak to appear at an energy somewhat greater than 184 keV, as seen in Fig. 8. The size of the crystal is reflected in the relative areas under the total energy peak and the continuous distribution to its left. The larger the detector, the more often it captures the total energy of an incident photon, thus diminishing the size of the continuum and enhancing the size of the peak.

An additional feature in gamma-ray pulse-height spectra, not possible with ^{137}Cs, can be found when the energy of the incident photons exceeds the threshold, 1.022 MeV, for pair production. The incident photons can then produce electron-positron pairs with total initial kinetic energy $T_- + T_+ = h\nu - 2mc^2$. Both stop quickly in the crystal, contributing this amount of energy toward the resulting pulse. The stopped positron also annihilates rapidly with an electron, creating two 0.511-MeV back-to-back photons. If both annihilation photons are absorbed in the crystal, then the resulting pulse will be registered in the peak centered at $h\nu$, the incident photon energy. If one or both annihilation photons escape the detector, then the pulse will be registered at either $h\nu - 0.511$ MeV or $h\nu - 1.022$ MeV. The spectral peaks at energies mc^2 or $2mc^2$ below the total energy peak are called *escape peaks*.

NEUTRON INTERACTIONS

The strong force

The neutron is a neutral particle with a mass and size comparable to the proton. It is a normal constituent of atomic nuclei and, like the proton, also binds with other nucleons by means of the strong, or nuclear, force. The neutron interacts with matter only through this force, which has a very short range of the order of 10^{-15} m. [At extreme relativistic energies, additional forces between the neutron and electron, involving their spins, magnetic moments, and the internal structure of the neutron, come into play (Turner et al. 1973).] In the picture of the Rutherford nuclear atom described earlier, a neutron can travel a considerable distance through many atoms without having a collision. It has an encounter only when it gets within the short range of the strong force of an atomic nucleus—a small target.

For convenience, neutrons can be classified loosely according to their energies. *Thermal* neutrons are in approximate thermal equilibrium with their surroundings. They have a Maxwell-Boltzmann energy distribution with a maximum at 0.025 eV at room temperature. *Cold* neutrons also exist at lower temperatures. Thermal neutrons diffuse about, losing and gaining small amounts of energy until they are eventually captured by a nucleus. A free neutron also decays radioactively with a half-life of 12 min by emission of a beta particle. Neutrons with energies up to 10 keV to 100 keV are variously called *slow*, *intermediate*, or *resonance*. *Fast* neutrons generally refer to those with higher energies.

A neutron can react with a nucleus in different ways. The principal mechanisms of importance here are nuclear reactions, which are inelastic, and nuclear elastic scattering.

Nuclear reactions

Nuclear reactions can occur when a neutron comes into close proximity with an atomic nucleus. (Protons can

similarly cause nuclear reactions, but they must first have sufficient kinetic energy in order to overcome the Coulomb force that repels them from the nucleus. Being neutral, the neutron faces no repulsive Coulomb barrier before entering the nucleus.) The following nuclear reactions are important for neutron detection, dosimetry, and health physics.

^{1}H(n,γ)^{2}H. Thermal neutrons are captured by ordinary hydrogen atoms with a cross section of 3.3×10^{-29} $m^2 = 0.33$ barns. A gamma ray of energy 2.22 MeV, representing the binding energy of the deuteron, is released from the nucleus upon capture. As typical of other thermal-neutron capture reactions, the cross section falls off with increasing energy as the reciprocal of the neutron velocity (the "$1/v$" law). Since they have little kinetic energy, when thermal neutrons irradiate soft tissue their sole mode of delivering an appreciable dose is by means of secondary products from capture reactions. A body absorbing thermal neutrons is thus exposed to the 2.22-MeV gamma radiation produced from capture of the neutrons by the hydrogen in tissue, which is very abundant. This process and the reaction ^{14}N(n,p)^{14}C, discussed below, are the only two of consequence for thermal-neutron dose.

^{3}He(n,p)^{3}H. This reaction, which has a capture cross section of 5,330 barns for thermal neutrons, releases an energy of 765 keV to the proton and triton produced. In addition to detecting thermal neutrons, ^{3}He is employed widely for fast-neutron detection and dosimetry. It is a good proportional-counter gas. An idealized pulse-height spectrum, measured for monoenergetic neutrons of energy E, would display a total-energy peak at $E + 765$ keV due to neutrons that are absorbed. In addition, the spectrum would show a continuum of pulses produced by ^{3}He recoil nuclei from which incident neutrons are elastically scattered. The continuum would extend from low energies up to $(3/4)E$, as given by eqn (12) when $M = 1$ and $m = 3$. In practice, a considerable fraction of the recoil charged particles might encounter the chamber walls before their energy is spent in ionizing the gas. Such wall effects also occur in other types of proportional counters. In addition, an epithermal peak at 765 keV will result from fast neutrons that are moderated by surrounding objects and nearly thermalized before entering the counter.

^{6}Li(n,t)^{4}He. This reaction, which releases 4.78 MeV, is also important for thermal-neutron instrumentation. The cross section for thermal capture is 940 barns. LiI scintillators can be made with lithium enriched in ^{6}Li (natural abundance 7.42%), for low-energy neutron detection. ^{6}Li can also be added to other detectors to make them neutron sensitive. LiF is very important for thermoluminescence dosimetry (TLD). With constituents of low atomic number, it is reasonably tissue equivalent. Similar TLD chips of essentially pure ^{6}LiF and pure ^{7}LiF show the same response when exposed together to a gamma source. They show a different response when exposed to neutrons. The ^{6}LiF chip responds to neutrons; ^{7}LiF is insensitive to them. Comparison of the two calibrated chips permits assessment of the separate gamma and neutron doses.

^{10}B(n,α)^{7}Li. The thermal-neutron capture cross section is 3,840 barns, and the energy release is either 2.31 MeV or 2.79 eV, depending on whether neutron capture leaves the ^{7}Li nucleus in an excited state (96%) or in its ground state (4%). BF_3 is used as a proportional-counter gas. It can be enriched in ^{10}B above its natural 19.7% abundance. Some counters monitor slow neutrons directly. Others are surrounded by a moderating material and used to monitor fast neutrons. The fast neutrons slow down in the moderator and are captured as slow neutrons by the boron. No information is gained, however, about the neutron spectrum. Basically, these counters can screen out pulses due to gamma rays through amplitude discrimination. Gamma photons produce secondary electrons in the counter walls and gas. These are low-LET secondaries with relatively long ranges, typically crossing the counter gas with little production of ionization. Neutron capture, in contrast, releases the densely ionizing alpha particles and ^{7}Li recoil nuclei, producing a relatively large number of ions.

^{14}N(n,p)^{14}C. This reaction has a thermal-neutron capture cross section of 1.70 barns and releases 0.626 MeV. Together with the ^{1}H(n,γ)^{2}H capture reaction described above, it is the second of the two reactions that result in dose to tissue from exposure to thermal neutrons. Whereas the energy released in hydrogen capture is transported away from the capture site by the energetic photon emitted, the charged particles from capture by nitrogen deposit their energy in the immediate vicinity of the capture site.

^{23}Na(n,γ)^{24}Na. Absorption of a neutron by normal ^{23}Na (100% abundant) produces the beta emitter ^{24}Na. This isotope has a half-life of 15.0 h. It emits beta particles with an average energy of 0.554 MeV and two gamma rays (1.369 MeV and 2.754 MeV) with 100% frequency. The thermal-neutron capture cross section is 0.534 barns. This reaction is potentially relevant for

detecting activated blood sodium in persons exposed to high levels of neutrons, as in a criticality accident.

^{32}S(n, p)^{32}P. This is an example of an endothermic threshold reaction. It is energetically impossible unless the neutron has an energy of at least 0.957 MeV. Above this threshold, however, the cross section increases slowly with energy. The reaction becomes practical for detection of neutrons only at energies above about 3.2 MeV. ^{32}P is a pure beta emitter with an average energy of 0.695 MeV and a half-life of 14.3 d. Activation of ^{32}S (95% abundant) in human hair can provide information on exposure of individuals to fast neutrons. Sulfur is included as one of several elements in threshold neutron detectors. These detectors consist of foils of various elements, having different energy thresholds for activation. After exposure to a neutron field, the measured activities of the different foils can be used to help infer the neutron energy spectrum.

^{113}Cd(n, γ)^{114}Cd. The thermal-neutron capture cross section is a very large 21,000 barns. It remains large up to about 0.2 eV, and drops off to much lower values below the so-called "cadmium cutoff" at ~0.4 eV. Cadmium is widely used for neutron shielding and reactor control rods. ^{113}Cd is 12.3% abundant.

^{115}In(n, γ)^{116m}In. The thermal-neutron capture cross section for ^{115}In (95.7% abundant) is 157 barns, and the half-life of the metastable ^{116m}In is 54.2 min. Almost the entire thermal-neutron capture cross section is due to the resonance at 1.46 eV. Activity detected in indium foils worn by personnel could be potentially useful as evidence of exposure to neutrons following an accident.

^{197}Au(n,γ)^{198}Au. ^{197}Au (100% abundant) can be used for slow-neutron detection. The thermal capture cross section is 98.8 barns. The half-life of the beta emitter ^{198}Au is 2.70 d.

^{235}U(n, f). The huge energy release from fission (f) following capture of a thermal neutron by ^{235}U provides a distinct feature for their detection, even in fields of high background.

Elastic scattering

Elastic scattering occurs when a neutron collides with a nucleus and there is no change in the total kinetic energy of the two. An initially stationary nucleus recoils with initial kinetic energy exactly equal to the amount of kinetic energy that the neutron loses. If the total kinetic energy of the two is reduced, as in a nuclear reaction or resonance scattering, then the collision is inelastic. In either instance, the total momentum is always conserved.

Among all of the chemical elements, hydrogen is special because the neutron and proton have virtually the same mass. Ordinarily, the struck nucleus is initially at rest. Then, with $M = m$ in eqn (12), the maximum possible energy transfer is E, the entire kinetic energy of the incident neutron. Hydrogen is the only atom that can stop a fast neutron in a single collision. Hydrogen also has a large scattering cross section and is very plentiful in the human body. The water content of the 73-kg ICRP Reference Man is 43 kg (ICRP 2002). In addition to its special importance in neutron and reactor physics, hydrogen plays a special role in radiation dosimetry.

As mentioned above, the absorbed dose in tissue from slow neutrons is generated by the energy released from their nuclear-capture reactions in tissue. Energetic neutrons, on the other hand, undergo relatively little nuclear reactions. They deposit dose by direct transfer of kinetic energy to tissue nuclei through elastic collisions. Most of the fast-neutron dose to soft tissue comes from the proton recoils in hydrogen collisions. Table 1 shows the fraction of the total neutron kerma that is due to scattering from hydrogen at different neutron energies. The remainder of the kerma comes from the combined contributions of scattering by carbon, oxygen, and nitrogen (NBS 1961).

Neutron-proton elastic scattering has some interesting properties. Consider a neutron with initial kinetic energy E incident on a proton initially at rest, and assume equal masses M for the two. Let the vectors $\boldsymbol{V}$ and $\boldsymbol{V}'$ represent the neutron's velocity before and after collision, and $\boldsymbol{\nu}'$ be that of the recoil proton. Momentum conservation requires that the vectors form a triangle such that

$$M\boldsymbol{V} = \mathrm{M}\boldsymbol{V}' + \mathrm{M}\boldsymbol{\nu}'. \quad (36)$$

Dividing by the mass leaves a triangle with the vector sides

$$\boldsymbol{V} = \boldsymbol{V}' + \boldsymbol{\nu}'. \quad (37)$$

Kinetic energy conservation for the elastic collision requires that

Table 1. Fraction of neutron soft-tissue kerma from collisions with hydrogen by neutrons of different energy.

Neutron energy (MeV)	Hydrogen fraction
0.01	0.97
0.10	0.96
1.00	0.83
10.0	0.85
14.0	0.76

$$\frac{1}{2}MV^2 = \frac{1}{2}MV'^2 + \frac{1}{2}M\nu'^2, \tag{38}$$

or $V^2 = V'^2 + \nu'^2$. This last relationship, applied to the sides of the triangle represented by eqn (37), implies that it must be a right triangle (Pythagorean theorem). That is, the neutron and proton always scatter in directions that are 90° apart after collision. Furthermore, if the proton is scattered at an angle θ with respect to the original direction of the neutron, then the energy it acquires is given by

$$Q = E\cos^2\theta. \tag{39}$$

The neutron is then scattered at an angle $90° - \theta$ with energy $E - Q$.

Like eqns (20)–(23) for Compton scattering, these relationships for neutron-proton scattering are kinematically required by the conservation laws, independently of the nature of the actual physical forces at work. The probability distributions for the events, however, are another matter. Their quantum-mechanical calculation depends specifically on distance, spin, and other details of the nuclear force. Experimentally, for neutrons with energies up to about 10 MeV, it is observed that neutron-proton scattering is isotropic in the center-of-mass coordinate system. That is, when viewed by an observer moving with the same velocity in the laboratory as the center of mass, the collision has the special property of isotropy. The neutron and proton recoil back-to-back from one another with equal likelihood in any direction. (Their speeds are also unchanged by the elastic collision in this reference system.) As a result of isotropy in the center-of-mass system, the probability distribution for the proton-recoil energy Q in the laboratory system, shown by eqn (39), is flat. That is, all elastic energy losses for a neutron between 0 and the maximum of E are equally likely. It thus follows that, in a collision with hydrogen, the neutron loses an average of one-half its kinetic energy, $E/2$.

Some health physics aspects

Sometimes rough, back-of-the-envelope estimates of the dose from fast neutrons are useful. An approximation to the first-collision dose in tissue can be made by considering only first collisions with hydrogen in a water phantom. The neutron scattering cross section with hydrogen varies from about 5 barns at 1 MeV to 1 barn at 10 MeV. Assuming a cross section $\sigma = 2$ barns $= 2 \times 10^{-28}$ m^2 for neutrons in this energy range will not be far off. The number of hydrogen atoms per unit mass of water is $N = 6.69 \times 10^{25}$ kg^{-1}. Neutrons of energy E transfer an average energy of $E/2$ in a collision with hydrogen. If the neutron fluence is Φ (m^{-2}), then the first-collision dose in water from collisions with hydrogen alone is $D = (\Phi N\sigma)(E/2)$. Substituting the given numerical values and, for convenience, letting $E = E_{\mathrm{MeV}}$ represent the incident-neutron energy in MeV, one obtains for the dose per unit fluence

$$\frac{D}{\Phi} = 1.1 \times 10^{-15}\, E_{\mathrm{MeV}}\ \mathrm{Gy\ m^2}. \tag{40}$$

At 2 MeV, as an example, this estimate of the first-collision dose per unit fluence in water from hydrogen scattering alone is 2.2×10^{-15} Gy m^2. Detailed calculation of the first-collision dose for 2-MeV neutrons in soft tissue, considering all elements, gives 3.00×10^{-15} Gy m^2 (NBS 1961). The simple formula (eqn 40) provides a reasonable first approximation to tissue dose from fast neutrons. However, no allowance is made for multiple neutron scattering or for predicting the absorbed dose as a function of depth.

The quantity calculated by means of eqn (40) is actually kerma. It is a good approximation to absorbed dose under conditions of charged-particle equilibrium. For photons, eqn (35) related the kerma to the energy fluence Ψ and the mass energy-transfer coefficient. For neutrons, it is more common to relate the kerma to the neutron fluence Φ, rather than energy fluence. In place of eqn (35) and the mass energy-transfer coefficient used for monoenergetic photons, one then writes the kerma for monoenergetic neutrons as $K = \Phi F$, in which F is called the *kerma factor*. The kerma per unit fluence, K/Φ, is also termed the *kerma coefficient* (ICRU 1998). It depends on the neutron energy and on the material of the absorber. Tables of neutron kerma factors are available in the literature (Caswell et al. 1980; Attix 1986). For 2-MeV neutrons in water, one finds (Attix 1986) $K/\Phi = 3.3 \times 10^{-9}$ rad cm^2. This value converts to 3.3×10^{-15} Gy m^2. It can be compared with the above estimate, 2.2×10^{-15} Gy m^2, based on eqn (40). For tissue, the kerma factor for 2-MeV neutrons is 3.0×10^{-15} Gy m^2.

A proposed rule of thumb for dose equivalent in a field of approximately 2-MeV neutrons is

$$H(\mathrm{rem/hr}) \cong 1.4 \times 10^{-4}\varphi, \tag{41}$$

where the fluence rate is φ neutrons cm^{-2} s^{-1} (Shleien et al. 1998). With an assumed quality factor of 10 (NCRP 1971), this rule implies that $D/\Phi \cong 3.9 \times 10^{-15}$ Gy m^2, consistent with the order of magnitude of the rough approximation (eqn 40).

Dating back to the 1950's, the reaction $^{10}\mathrm{B}(n,\alpha)^7\mathrm{Li}$, utilized in some neutron detectors, has been the basis for the exploration of *boron capture therapy* directed toward cancer treatment. The idea is to administer a boron-containing drug into a tumor and then irradiate it with

thermal neutrons. The neutrons selectively deliver a large, localized dose in the tumor from the high-LET ions produced as a result of their capture by the boron. Tissues that do not have the boron are spared by comparison. While the principle continues to be explored, a number of formidable obstacles remain standing in the way of practical clinical treatments. Extensive information about boron capture therapy can be found on the World Wide Web.

CONCLUDING THOUGHTS

This review has focused largely on the interaction of radiation with individual atoms and nuclei. While addressing the central theme of the subject, some additional aspects will be mentioned in conclusion.

Radiation interactions in the condensed phase

In some condensed materials, the positions of electrons are correlated over much larger distances than the separation of the atoms. The medium cannot then be regarded strictly as an assembly of individual, independent atoms with respect to its interaction with radiation. The passage of a charged particle polarizes the medium, thereby reducing the stopping power. In addition to the theory as presented above, one must include interactions in which the energy transferred is shared among large numbers of electrons and ions, acting collectively in the condensed state. The dynamic response of the medium can be characterized by a complex dielectric function, which governs the energy loss. The change in stopping power due to the density effect is usually small unless the kinetic energy of the ion is comparable to or greater than its rest energy (Fano 1963; Ritchie et al. 1991; ICRU 1993a).

Dosimetry

Understanding radiation interactions is essential for measuring absorbed dose. Attix (1986) has defined a dosimeter "generally as any device that is capable of providing a reading r that is a measure of the absorbed dose D_g deposited in its *sensitive volume V* by ionizing radiation." He goes on to say, "Interpretation of a dosimeter reading in terms of the desired quantity is the central problem in dosimetry, usually exceeding in difficulty the actual measurement."

To illustrate, cavity ionization chambers that satisfy Bragg-Gray conditions have been designed and constructed for measuring dose and dose rate for gamma rays and neutrons. Basically, such an instrument can provide the absorbed dose in the wall material of the chamber from measurement of the ionization produced in the cavity gas. However, specific conditions must be met in order to achieve this relationship. One must deal with such matters as proper wall thickness and charged-particle equilibrium, details of charge collection in the gas, dose discontinuity at the wall/gas and gas/wall interfaces, energy-dependent secondary charged-particle spectra in the wall and gas, as well as other factors. These technical requirements are examined carefully and met at standards laboratories that perform calibrations. Only through traceability back to these rigorous conditions, can there be confidence in what a reading r of Attix's dosimeter is really telling one.

The Bragg-Gray principle, which is the basis for much of dosimetry, relates the ionization in one component of a test system (cavity) to the energy absorbed in another component (wall). A generalized approach to radiation dosimetry has been formulated by Hurst and Ritchie (1962). Their dosimeter comprises special electronic circuits that operate on the energy-loss distributions resulting from the interactions of radiation with the detector. The response of the detector is designed to have nearly the same dependence on radiation energy as the system in which the dose is desired. The authors present several applications of the generalized approach.

Radiation quality and dose

This final section speculates briefly from the standpoint of radiation interactions about the familiar, related concepts of radiation quality and dose.

In NCRP Report No. 104 (NCRP 1990), "The term 'radiation quality' . . . refers to the energy imparted to matter divided by the length of the track of the charged particle over which the energy is lost." Of the various quantities that approximate this definition, LET is the parameter most often employed to indicate expected biological effectiveness. Other quantities, such as restricted LET or the stochastic *lineal energy, y*, from the field of microdosimetry (ICRU 1983, 1993b; Rossi and Zaider 1996) have also been considered. All are related to stopping power and have the same dimensions.

At a more fundamental level than LET, the inelastic scattering cross section for a charged particle expresses the *probability of interaction* per unit distance traveled. This can be contrasted with LET, which is the mean rate of energy loss per unit distance, as determined by the cross section. Theoretical arguments indicate that the physical properties of the radiation that determine cross section are charge and velocity, rather than LET (Turner and Hollister 1965). It can also be argued that properties of the biological targets themselves must be equally relevant (Katz 1994).

In principle, radiation dose could be defined to include other physical quantities besides energy absorbed per unit mass. That is not to say that other quantities would have the practical advantage that energy offers in

the relative ease of its measurement. However, as a predictor of biological effects, the energy absorbed per unit mass often needs to be supplemented by an empirical value for the RBE. It is interesting see whether one could define dose in a way that might obviate the need for such a factor.

One study toward this end explored the use of the magnitude of the momentum absorbed per unit mass for a series of neutron RBE experiments with mice (Turner and Hollister 1962). Data were assembled from a number of laboratories by Bond and Bateman (1960). They presented RBE as a function of neutron energy from 0.4 MeV to 13 MeV for lethality and spleen, thymus, and intestinal weight loss. The variation of RBE with neutron energy for these different endpoints was about the same. The RBE was linear on a semi-log plot, ranging from a high of 4.6 down to 1.5 with increasing neutron energy. In the analysis, a number of potential dose parameters involving the energy and momentum absorbed per unit mass, E_{abs} and P_{abs}, were explored. It was found that the following "dose" remained constant to within about $\pm 10\%$ over the range of neutron energies that encompass the data:

$$\omega = \alpha_1 E_{abs} + \alpha_2 P_{abs} = \frac{E_{abs}}{100} \left(0.94 + 1.4 \times 10^9 \frac{P_{abs}}{E_{abs}}\right). \quad (42)$$

Here the energy and momentum absorbed per unit mass are in cgs units, and the constants α_1 and α_2 were determined numerically by least-squares fitting of the data. The term $E_{abs}/100$ in erg g^{-1} is the absorbed dose in rad. The factor in parentheses appears formally in the role of RBE. It multiplies the absorbed dose, keeping the dose ω at a fixed level as the neutron energy is varied.

To compare with the customary reference radiation for RBE, ω as given by eqn (42) was applied to photons. The second term in parentheses then turns out to be negligible, leaving only the factor 0.94 as the RBE of photons of any energy. The requirement that a new dose parameter apply to all types of radiation does not appear to be trivial. A convenient feature of ω is its linear dependence on the two physical quantities. Having this property, it would be applicable to neutrons with arbitrary energy spectra and to mixed gamma-neutron fields.

One can understand how the linear combination of energy and momentum expressed by eqn (42) might be expected to mimic the RBE. Neutrons transfer their energy primarily to atomic nuclei by elastic scattering. In contrast, photons transfer their energy to the much less massive electrons. The amount of momentum absorbed per unit of energy absorbed is much larger if the targets are massive, and the efficiency increases with decreasing neutron energy. The recoil nuclei are densely ionizing.

Years ago, Failla and Marinelli (1937) described the great difficulty of measuring gamma rays in terms of the roentgen. They spoke of the desirability of having a single quantity that could serve to correlate with tissue and biological effects in therapy. Since that time, techniques for measuring other quantities for different radiations have advanced enormously. The premise that new definitions of radiation dose might be important should perhaps be revisited with today's digitalized technology.

REFERENCES

Attix FH. Introduction to radiological physics and radiation dosimetry. New York: Wiley & Sons; 1986.

Bethe H. Zur Theorie des Durchgangs schneller Korpuskularstrahlen durch Materie. Ann der Phys 5:325–400; 1930 (in German).

Bethe H. Handbuch der Physik 24(1). Berlin: Springer; 1933 (in German).

Bloch F. Bremsvermogen von Atomen mit mehreren Elektronen. Zeits fur Phys 81:363–376; 1933 (in German).

Bohr N. On the theory of the decrease of velocity of moving electrified particles on passing through matter. Phil Mag 25:10–31; 1913a.

Bohr N. On the constitution of atoms and molecules. Phil Mag 26:1–25; 1913b.

Bohr N. On the constitution of atoms and molecules. Phil Mag 26:476–502; 1913c.

Bohr N. On the decrease of velocity of swiftly moving electrified particles in passing through matter. Phil Mag 30:581–612; 1915.

Bond VP, Bateman JL. Relative biological effectiveness. Statement prepared for hearings of the Joint Committee on Atomic Energy, May 25–June 3, 1960. In: Radiation protection criteria and standards: their basis and use. Washington, DC: U.S. Government Printing Office; 1960.

Caswell RW, Coyne JJ, Randolph ML. Kerma factors for neutron energies below 30 MeV. Rad Res 83:217–254; 1980.

Cember H. Introduction to health physics. New York: McGraw-Hill; 1996.

Dirac PAM. The quantum theory of the electron. Proc Roy Soc (London) A117:610–624; 1928.

Dirac PAM. The principles of quantum mechanics. New York: Oxford, UK; 1958.

Durham JS, Bell JM. VARSKIN MOD 2 and SADDE MOD 2: Computer codes for assessing skin dose from skin contamination. Springfield, VA: National Technical Information Service; NUREG/CR-5873; 1992.

Evans RD. Gamma rays. In: Gray DE, ed. American Institute of Physics handbook. New York: McGraw-Hill; 1972:8–190 to 8–218.

Evans RD. The atomic nucleus. Malabar, FL: Krieger; 1985. Reprint of original, New York: McGraw-Hill; 1955.

Failla G, Marinelli, LD. Ionisation in air by gamma-rays. Am J Roent Radium Therapy 38:312–343; 1937.

Fano U. Penetration of protons, alpha particles, and mesons. Ann Rev Nucl Sci 13:1–66; 1963.

Fermi E. Nuclear physics. Chicago, IL: Chicago; 1950.

Feynman RP. QED: the strange story of light and matter. Princeton, NJ: Princeton; 1985.
Geiger H, Marsden E. On a diffuse reflection of the alpha-particles. Proc Roy Soc (London) A82:495–500; 1909.
Hall EJ. Radiobiology for the radiologist. Philadelphia, PA: Lippincott, Williams & Wilkins; 2000.
Heisenberg W. Uber quantentheoretische Umdeutung kinematischer und mechanischer Beziehungen. Zeit fur Phys 33:879–893; 1925 (in German).
Hubbell JH. Review of photon interaction cross section data in the medical and biological context. Phys Med Biol 44:R1–R22; 1999.
Hurst GS, Ritchie RH. A generalized concept for radiation dosimetry. Health Phys 8:117–129; 1962.
ICRP. 1990 recommendations of the International Commission on Radiological Protection. Oxford, UK: International Commission on Radiological Protection; ICRP Publication 60; 1991.
ICRP. Basic anatomical and physiological data for use in radiological protection: reference values. Oxford, UK: International Commission on Radiological Protection; ICRP Publication 89; 2002.
ICRU. Radiation quantities and units. Bethesda, MD: International Commission on Radiation Units and Measurements; ICRU Report 33; 1980.
ICRU. Microdosimetry. Bethesda, MD: International Commission on Radiation Units and Measurements; ICRU Report 36; 1983.
ICRU. Stopping powers for electrons and positrons. Bethesda, MD: International Commission on Radiation Units and Measurements; ICRU Report 37; 1984.
ICRU. Stopping powers and ranges for protons and alpha particles. Bethesda, MD: International Commission on Radiation Units and Measurements; ICRU Report 49; 1993a.
ICRU. Quantities and units in radiation protection dosimetry. Bethesda, MD: International Commission on Radiation Units and Measurements; ICRU Report 51; 1993b.
ICRU. Dosimetry of external beta rays for radiation protection. Bethesda, MD: International Commission on Radiation Units and Measurements; ICRU Report 56; 1997.
ICRU. Fundamental quantities and units for ionizing radiation. Bethesda, MD: International Commission on Radiation Units and Measurements; ICRU Report 60; 1998.
Kathren RL, Ziemer PL. The first fifty years of radiation protection. In: Kathren RL, Ziemer PL, eds. Health physics: A backward glance. Elmsford, NY: Pergamon; 1980: 1–9.
Katz R. Dose. Rad Res 137:410–413; 1994.
Klein O, Nishina Y. Uber die Streuung von Strahlung durch freie Elektronen nach der neuen relativistischen Quantendynamik von Dirac. Zeit für Phys 52:853–868; 1929 (in German).
Morgan KZ. History of damage and protection from ionizing radiation. In: Morgan KZ, Turner JE, eds. Principles of radiation protection. New York: Wiley & Sons; 1967: 1–75.
NAS. Health risks of radon and other internally deposited alpha emitters (BEIR IV). Washington, DC: National Academy of Sciences; 1988.
NBS. Measurement of absorbed dose of neutrons and mixtures of neutrons and gamma rays. Washington, DC: National Bureau of Standards; Handbook 75; 1961.
NCRP. Protection against neutron radiation. Bethesda, MD: National Council on Radiation Protection and Measurements; NCRP Report No. 38; 1971.
NCRP. The relative biological effectiveness of radiations of different quality. Bethesda, MD: National Council on Radiation Protection and Measurements; NCRP Report No. 104; 1990.
NCRP. Limitation of exposure to ionizing radiation. Bethesda, MD: National Council on Radiation Protection and Measurements; NCRP Report No. 116; 1993.
NCRP. Biological effects and exposure limits for "hot particles." Bethesda, MD: National Council on Radiation Protection and Measurements; NCRP Report No. 130; 1999.
Parker HM. Health physics, instrumentation, and radiation protection. Health Phys 38:957–996; 1980. Reprinted from Adv Biol Med Phys; 1948.
Ritchie RH, Hamm RN, Turner JE, Wright HA, Bolch WE. Radiation interactions and energy transport in the condensed phase. In: Glass WA, Varma MN, eds. Physical and chemical mechanisms in molecular radiation biology. New York: Plenum; 1991: 99–134.
Rossi HH, Zaider M. Microdosimetry and its applications. Berlin, Germany: Springer; 1996.
Rutherford E. On the scattering of alpha and beta particles by matter and the structure of the atom. Phil Mag 21:669–688; 1911.
Rutherford E. Background in modern science. New York: Macmillan; 1938.
Schrodinger E. Quantizierung als Eigenwertproblem. Ann der Phy 79:361–376; 1926a (in German).
Schrodinger E. Quantizierung als Eigenwertproblem. Ann der Phy 79:489–527; 1926b (in German).
Schrodinger E. Uber das Verhältnis der Heisenberg-Born-Jordanschen Quantenmechanik zu der meinen. Ann der Phy 79:734–756; 1926c (in German).
Seltzer SM, Berger MJ. Bremsstrahlung energy spectra from electrons with kinetic energy 1 keV–10 GeV incident on screened nuclei and orbital electrons of neutral atoms with Z = 1–100. At Data and Nucl Data Tables 35:345–418; 1986.
Semenenko VA, Turner JE, Borak TB. NOREC, a Monte Carlo code for simulating electron tracks in liquid water. Rad Env Biophys 42:213–217; 2003.
Shleien B, Slaback LA, Birky BK. Handbook of health physics and radiological health. Baltimore, MD: Williams and Wilkins; 1998.
Stannard JN. Radioactivity and health. A history. Springfield, VA: National Technical Information Service; 1988.
Taylor LS. Who is the father of health physics? Health Phys 41:91–92; 1982.
Turner JE, Hollister H. The possible role of momentum in radiation dosimetry. Health Phys 8:523–532; 1962.
Turner JE, Hollister H. Relationship of the velocity of a charged particle to its relative biological effectiveness. Nature 208:36–37; 1965.
Turner JE. Calculation of stopping power of a heavy charged particle. Health Phys 13:1255–1263; 1967.
Turner JE, Kher RK, Arora D, Bisht JS, Neelavathi VN, Vora RB. Quantum mechanical calculation of neutron stopping power. Phys Rev B 8:4057–4062; 1973.
Turner JE, Paretzke HG, Hamm RN, Wright HA, Ritchie RH. Comparative study of electron energy deposition and yields in water in the liquid and vapor phases. Rad Res 92:47–60; 1982.
Turner JE, Hamm RN, Souleyrette ML, Martz DE, Rhea TA, Schmidt DW. Calculations for beta dosimetry using Monte Carlo code (OREC) for electron transport in water. Health Phys 55:741–750; 1988.
Turner JE. Atoms, radiation, and radiation protection. New York: Wiley & Sons; 1995.
Weisskopf VF. The privilege of being a physicist. New York: W. H. Freeman & Co.; 1989.

■ ■